Atmos. Chem. Phys. Discuss., 7, 11895–11971, 2007
www.atmos-chem-phys-discuss.net/7/11895/2007/
© Author(s) 2007. This work is licensed
under a Creative Commons License.

Atmospheric Chemistry and Physics Discussions

A comprehensive modelling way for assessing real-time mixings of mineral and anthropogenic pollutants in East Asia

F. Lasserre[1], G. Cautenet[1], C. Bouet[1], X. Dong[2], Y. J. Kim[3], N. Sugimoto[4], I. Matsui[4], and A. Shimizu[4]

[1]Laboratoire de Météorologie Physique, Université Blaise Pascal, Complexe scientifique des Cézeaux, BP 45, 63170, Aubière, France
[2]Sino-Japan Friendship Center for Environmental Protection, Beijing 100029, China
[3]Advanced Environment Monitoring Research Center, Department of Environmental Science and Engineering, Gwangju Institute of Science and Technology, 1 Oryong-dong, Gwangju 500-712, Korea
[4] National Institute for Environmental Studies, 16-2 Onogawa, Tsukuba, Ibaraki 305-8506, Japan

Received: 4 June 2007 – Accepted: 8 August 2007 – Published: 14 August 2007

Correspondence to: G. Cautenet (g.cautenet@opgc.univ-bpclermont.fr)

Abstract

In order to assess the complex mixing of atmospheric anthropogenic and natural pollutants over the East Asian region, we propose to take into account the main aerosols simultaneously present over China, Korea and Japan during the spring season. With the mesoscale RAMS (Regional Atmospheric Modeling System) tool, we present a simulation of natural (desert) dust events along with some of the most critical anthropogenic pollutants over East Asia: sulphur elements (SO_2 and SO_4^{2-}) and Black Carbon (BC).

During a 2-week case study of dust events which occurred in April 2005 over an area extending from the Gobi deserts to the Japan surroundings, we retrieve the behaviours of the different aerosols plumes. We focus on possible dust mixing with the anthropogenic pollutants from megalopolis. For both natural and anthropogenic pollution, the model results are in general agreement with the horizontal and vertical distributions of concentrations as measured by remote data, in situ LIDAR, PM_{10} data and literature. In particular, we show that a simplified chemistry approach of this complex issue can be efficient enough to model this event, with a real-time step of 3 h. The model provides the good shapes and orders of magnitude for the Aerosol Optical Thickness (AOT) and species contributions (via the Angström Exponent) when compared with the AERONET data.

1 Introduction

Anthropogenic pollution is a permanent element of the climate over Asian megalopolis and surrounding countries. Moreover, these areas are also subject to natural pollutions from mineral origin, when a dust desert storm occurs (Sun et al., 2001). Thus, mainly at spring, aerosols plumes from natural and anthropogenic origins can coexist over northern China, Korea and Japan. According to Tang et al. (2004), mesoscale simulations of heterogeneous reactions in the boundary layer show an average decrease of 55% in SO_2 content when mixed with dust (ACE-Asia (Asian Pacific Regional Aerosol

ACPD

7, 11895–11971, 2007

Characterization Experiment), April 2001). In severe dust storm conditions, the sulphate production would increase by 20% in the coarse mode. This example among others shows that it is necessary to take the anthropogenic aerosol into account along with the natural aerosol in order to have a correct sight of the Asian aerosol cycle.

For the sandstorms which occurred at Beijing in spring and summer 2000, Liu et al. (2005) provided microscopic analyses and chemical characterization of the mineral dust and particles containing sulphur elements. These analyses detailed the extreme difficulty of the "inversion" work which consists in seeking the weather conditions, as Relative Humidity (RH) and cloud cover, for conversion of SO_2 gas into sulphur products. It is also true for carbonaceous soot mixed with mineral dust: see, for example, Shi et al. (2003) in Beijing. Black Carbons (BC) are products of industrial activity, fuel particles, residues of agricultural or forest fires and incomplete domestic combustions of coal and biomass. BC emissions are particularly important in China where cooking and heating are often based upon wood, vegetable cracks, dung or coal, at too low temperatures to achieve complete combustions. Mixed with other emitted pollutants in the vicinity (e.g. organic carbons), BC can form what is commonly called "black soot".

Presence of BC particles in the air does not induce only a harmful pollution as regards human health, it also affects the atmospheric processes: physical (direct and indirect effects), chemical (as sufficiently subdivided elements, they support $SO_2 \rightarrow SO_4^{2-}$ conversion (Novakov et al., 1974)) and photochemical as well. BC aerosols are consequently subjects of studies in order to preserve public health and to better understand regional and global climatic changes (Chylek et al., 1995; Jacobson, 2001; Menon et al., 2002).

The objective of this article is to assess a comprehensive way to analyze the compared roles of the main anthropogenic pollutants in the total pollution. We therefore voluntary simplify the problem and we consider a very restricted number of anthropogenic pollutants to only retain some of the most representative ones: sulphur compounds and BC.

We use a mesoscale model coupled with special modules which account for the

ACPD
7, 11895–11971, 2007

sources of natural (desert dust) and anthropogenic pollutants. We examine the atmospheric cycle of these pollutants over a few days, with a sufficiently short time step to take into account, "in real time", the strong variability of that kind of events. On a case study, we detail the possible interactions with the mineral aerosols carried by a sandstorm of "medium" intensity (i.e. the most standard events). Then, we compare the modelled plumes with remote (satellites, LIDAR) and surface data along with surface measurements of Atmospheric Optical Thickness (AOT). We also use, as much as possible, the available bibliography where observational data are not available.

With regard to the natural component of the studied event, we voluntarily do not seek to restore a situation which would correspond obviously to a tremendous storm like the storms of exceptional intensities of 19 April 1998 or 20 March 2002. The uploaded masses of these severe dust storms are of great interest, but, in frequency, they only represent a minor fraction of the events of mineral pollution. The sandstorm that we study is not as "spectacular" as those which are described preferentially in the literature, but it is certainly more difficult to model: it is challenging to deal with that kind of "ordinary" storm and to compare the instantaneous model outputs with observational data. Recall that these moderate sandstorms are responsible for most of the dusty days in China, as observed and modelled by Laurent et al. (2005).

After this introduction of our objectives, we will detail the model parameters in Sect. 2. As this simulation – like it is often the case with that kind of work – does not benefit of constraining data in all the places, at every moment and for all the considered species, this article is the opportunity to make a somewhat exhaustive review of the orders of magnitude for the pollutant concentrations and correlate effects and studies (Sect. 3 and others, for each opportunity of interest), whereas the quantitative data that we used to compare the modelled aerosol plumes with the observations are detailed in Sect. 4. Section 5 gives the different model results according to desert dust flux budgets and the resulting plumes, the anthropogenic plumes, the mixings between mineral dust and sulphur aerosols, the local studies over 2 Chinese cities representative of the aerosols pathways. We particularly detail the use of the AERONET (AErosol RObotic NETwork,

ACPD
7, 11895–11971, 2007

EGU

Holben et al., 1998) data (http://aeronet.gsfc.nasa.gov/) to validate the efficiency of our comprehensive approach of this complex issue.

2 The model tools

2.1 A short description of the RAMS mesoscale model

We use the mesoscale Regional Atmospheric Modeling System (RAMS) model developed by the Colorado State University (Cotton et al., 2003) in its 4.3 paralleled version. It is a eulerian, non-hydrostatic meteorological model featuring powerful facilities such as 4DDA (four dimensional data assimilation), interactive 2-way nesting (up to 8 grids), bulk or detailed microphysics (7 hydrometeors) and a comprehensive surface model. In order to accurately represent the aerosols cycles, we coupled RAMS with natural and anthropogenic aerosol schemes (sources/sinks), as described in Sects. 2.2, 2.3 and 2.4.

The model grid is centered on (40 N, 108 E) and extends (with stereopolar projection) from (26 N, 79 E), to (45 N, 145 E). There are 235 gripoints in longitude and 95 in latitude, with a grid size of 25 km. In the vertical, we have 30 levels, from surface to about 22 km in expanding size (including 10 vertical steps from surface to about 1.2 km). The simulation begins on 25 April 2005 (00:00 UTC) in order to give 48 h for the fields' initialization. The time step used in calculation is 10 s. This low value is necessary for the numerical stability due to the presence of severe reliefs (Tibet and Pamir) in the South and West of the modelled zone. Simulation is carried out on 64 paralleled processors and needs approximately 30 h in CPU.

2.2 Desert dust processing

As regards desert dust, the aerosol flux is provided by the Dust Production Model (hereafter referred to as DPM) developed by Marticorena and Bergametti (1995), Marticorena et al. (1997a, b) and by Alfaro et al. (1998), Alfaro and Gomes (2001). In this

ACPD
7, 11895–11971, 2007

DPM scheme (Marticorena et al., 1997a, b; Alfaro and Gomes, 2001), the dust flux at a given grid point is the consequence of all the contributions of the various soil natures which make up the surface represented by the point. At a given grid point, and for each soil nature, the dust flux is calculated using a set of physical parameters, the most important being the roughness and the percentage of erodibility. We have previously selected the parameters values as detailed in the study of a mineral dust storm which occurred in North Eastern China, during spring 2002 (Lasserre et al., 2005).

Our soils types map is recalled on Fig. 1. The surface map is brought up to date, in term of erodibility, according to the snow-cover at the end of April 2005. As the snow-covered zones are primarily limited to the reliefs, we actually obtain a map (Fig. 2) of the real erodibilities "overlayable" on the soil types map. On Fig. 2, we precise the zone hereafter called 1, 2 and 3. Zone 3 (38–50 N, 94–119 E) concerns the overall North East map, including zone 1 and zone 2, but also non emissive pixels.

The DPM has been coupled online to the RAMS model (*online* means that the wind speed used as DPM input is provided by the model itself). At every time step and grid point, the DPM calculates the amount of mobilized dust, which is redistributed in the first model levels. We use a spectral representation, i.e. the dust mass flux is redistributed over 20 size classes (20 discrete bins) with radius values ranging from 0.1 μm to 13 μm. The spectrum has three lognormal mass components with radii: 0.75 μm, 3.35 μm and 7.1 μm, and logarithmic standard deviations 1.7, 1.6 and 1.5. The respective weights of each mode in the initial spectrum, i.e. during the dust rise and before any deposition, are governed by the available kinetic energy of the saltating aggregates (Alfaro et al., 1998; Alfaro and Gomes, 2001). The mineral aerosol density is assumed to be 2650 kg m^{-3} (Marticorena and Bergametti, 1995). Each dust class is then diffused by turbulence, advected in the three dimensions and deposited by gravity (dry removal) or by wet removal. For all these processes except removal, we have used the built-in "inert tracer" facility of RAMS: this scheme provides advection and diffusion of any passive scalar.

The coupling of the dust scheme with RAMS is described in Cautenet et al. (2000),

ACPD
7, 11895–11971, 2007

Pradelle and Cautenet (2002), Minvielle et al. (2004a, b) and in Lasserre et al. (2005).

2.3 Anthropogenic particles inventories

2.3.1 Sulphur particles and black carbons in East Asia area

We voluntary limit the list of the anthropogenic pollutants to only two major chemical families: (i) the main sulphur compounds, that is sulphur dioxide SO_2 and its derivative products as gaseous H_2SO_4 and sulphate ions SO_4^{2-} (e.g. ammonium sulphates), all species thereafter referred to as "sulphates"; (ii) carbonaceous soots of all forms, members of the BC family.

Nitrogen oxides are reputed as major anthropogenic urban pollutants. However, for our approach, we don't consider them because of their short life time inside the free troposphere before being caught by atmospheric moisture (Kunhikrishnan et al., 2004). Moreover, their contribution to the total AOT is weak compared to those of the absorbing BC and the scattering sulphates (Trijonis et al., 1990; Watson et al., 2001; Reddy et al., 2005).

70% of the Chinese power needs are provided by combustion of poor quality coal (inclosing up to 5% sulphur) which generates considerable amounts of atmospheric SO_2. For the year 2000, Chinese government statistics evaluate at 20 Mt the country SO_2 emissions, with 85% directly linked with coal combustion (Yang et al., 2002). Such sulphur pollution severely impacts on the public health and contributes to the acid rain process, the consequences of which concern more than 30% of China.

Japan is also concerned by the sulphur pollution. The regional winds and the mean meteorological conditions over the Korean peninsula and the Japanese archipelago explain why these two areas are so dramatically under the influence of the continentally born pollutants. For example, Hatakeyama et al. (1995) have performed SO_2 airborne measurements over the Japan Sea during November 1992 and found some concentrations exceeding 10 ppb (approximately more than 25 $\mu g\,m^{-3}$), which certainly originated from Korea.

The BC mass production is by far less than the acidic pollutant mass emission. Thus, with Wang (2004), we agree with a minor role of the BC on the global temperature trend. On a regional scale however, as suggested by this author and the scientific community, BC becomes a major actor of the local radiative budget and the local meteorological dynamics. BC aerosol strongly absorbs the solar wavelengths. Consequently, BC increases the temperature of its atmospheric layer and decreases, on the same time, the surface solar radiation. The heated air makes the air surrounding more unstable, creating a favourable ascending convection, in particular in China, with the formation of clouds which, in turn, are likely to produce precipitations on the strongly polluted areas. This situation is observed in China but the opposite situation (desaturation of the layer and subsequent inhibition of the formation of the clouds) can be observed on the Indian sub-continent (Minvielle, 2003). To sum up, the BC has complex radiative effects (direct and semi-direct). Besides, these effects are associated with the indirect effects of other pollutants like sulphates causing, for example, an average reduction of 5% of the droplets radii and an increase in same percentage of the cloud water (Kristjánsson, 2002). The ascending polluted and wet air above coastal China tends to be balanced by subsidences of dry air in the North, what contributes to desertification of this part of China. These last years, the North of China suffered from frequent sandstorms, whereas southcoastal China underwent precipitations in increased quantities. Menon et al. (2002) see in the anthropogenic emissions of absorbing pollutants the principal cause of these regional climatic tendencies. Wu et al. (2004) quantified this double climatic impact in China, detailing how the Southern areas are more and more subject to rains reinforced by the BC and coupling this phenomenon with the drying of the Northern air masses. In term of direct effect, they calculated a maximum cooling of 1.5 K in the South of the Yangtze Kiang (Blue River) Delta.

ACPD
7, 11895–11971, 2007

2.3.2 Model Inventories for anthropogenic pollutants

During former works, we already used data bases of SO_2 and BC emissions, for example in simulations of INDOEX campaign (Minvielle et al., 2004a, b). We again use these databases. For SO_2, we use the EDGAR database (Emission Database for Global Atmospheric Research) available on http://www.mnp.nl/edgar/model/edgarv32/ acidifying/ (Olivier et al., 1996). For BC emissions, we use the GEIA database Global Emissions Inventory Activity) on http://www.geiacenter.org/ (with all references).

EDGAR database shows strong emissions of SO_2 around central China (South of the studied zone) as, for example, around Shangaï. A set of urban centres, roughly included inside a (32 N–37 N; 110 E–118 E) zone, give a annual average of SO_2 emission higher than 0.75×10^{-9} kg m^{-2} s^{-1}. The area between Dalian and Shenyang, in the North of the Bohai Sea, a zone of intense activity with industries and power plants, is estimated to be strongly emissive. In South Korea, Seoul is characterized by EDGAR as a very emissing place, just like the industrial port of Pusan in the South of the country.

Main BC emission areas are found at the same locations than SO_2 emitting zones: the principal urban centres and places of industrial activities, mining productions and power plants.

2.4 A simple physico-chemical approach

2.4.1 Sulphur to sulphate conversion

We suppose that sulphur emissions are SO_2 gas emissions. After being injected within the RAMS first level, sulphur mass will be ruled according to the processes illustrated in Fig. 3. Even if the major part of SO_2 remains "free", we model the part which is coated (adsorbed) onto the mineral aerosol (Adams et al., 2005). The one chemical conversion explicitly considered in our model is SO_2 into H_2SO_4 (gas conversion). H_2SO_4 is then supposed to be quickly transformed into SO_4^{2-} (sulphate), because of moisture

ACPD
7, 11895–11971, 2007

EGU

present in the air. We do not model, but we regard as very probable the direct oxidation (if the ambient temperature is sufficient) of SO_2 into sulphate after its adsorption by the mineral particles. This aspect of the joint cycle of the mineral and sulphated aerosols is, for example, detailed by Kulshrestha et al. (2003) for dry mixtures of SO_2 and dust over India. According to literature data (see below), we choose a dry conversion rate $SO_2 \rightarrow SO_4^{2-}$ of 1% per hour, with $d[SO_4^{2-}]=-1.5d[SO_2]$, where $d[SO_2]$ is the SO_2 mass converted into sulphates every time step. The 1.5 coefficient accounts for the molar mass ratio. Note that the rates of dry transformation of SO_2 into SO_4^{2-} derived from the literature range over more than one order of magnitude. For example, Cox (1974) estimates this rate at 1∼10% per hour in an urban plume. Eliassen and Saltbones (1975) estimate a rate of transformation of approximately 0.7% per hour. The evaluation by Alkezweeny and Powell (1977) from airborne measurements is about 10 to 12% per hour, in an atmosphere which can contain more water than the preceding studies. The MICS-ASIA working group (Carmichael et al., 2001) ran model intercomparisons of long range transports and SO_2 deposits in East Asia for January and May 1993. Within intermediate latitudes (35 N–45 N) the conversion rate for $SO_2 \rightarrow SO_4^{2-}$ conversion is close to $1.10^{-5}\,s^{-1}$, which corresponds to a transformation of 60% per day. Obviously, the implied processes are not only gas phase processes. Especialy, Carmichael et al. (2001), note that the predictions show disparities in the results of concentrations of both SO_2 and sulphates. For China, concentrations estimates easily vary with a factor of 10 from one model to another.

2.4.2 Anthropogenic aerosols deposits

The dry deposit of the sulphur compounds (except for those captured by dust, Sect. 2.4.3) is treated in a way similar to that recommended by Carmichael et al. (2001) in their modellings within MICS-ASIA. Models are particularly sensitive to the direct ratio between the wet deposit of sulphates and precipitations on the one hand, and the estimate of the dry deposit of SO_2 on the other hand. About the turbulent deposit rates,

ACPD
7, 11895–11971, 2007

EGU

Xu and Carmichael (1998) studied in detail the dry deposit rates of SO_2 and sulphates in Asia. Their model highlights a strong seasonal dependence as well as a daily variability, both linked, amongst others, with the nature of the subjacent surface of deposit. The dry diurnal deposition speed of SO_2 in summer would be 4–5 mm s^{-1} above the top of forests and meadows, 2 mm s^{-1} above the top of cultures and 8 mm s^{-1} above oceans, with values 2 to 3 times lower by night. Sulphates would have dry deposition speed which may fluctuate but lower than 1 mm s^{-1}. In this work, we choose a turbulent deposition velocity of 2 mm s^{-1} for SO_2.

The interaction of the aerosols with condensated water limits, in our case, to the washout processes because we estimate that rainout, if it could happen, influence only in a marginal way the mass assessment of free aerosols: we suppose that most of the aerosols captured by cloudy water will be released during the cloud evaporation. Thus, we only consider capture by rainwater. Observed rainfalls were weak during the modelled period. Nevertheless, we have taken the aerosol wet scavenging into account. In this work, we do not consider the conversion $SO_2 \rightarrow SO_4^{2-}$ by aqueous way. In their study of transport of primary and secondary pollutants above the China and Japan Seas, McNaughton et al. (2004) concluded that after 2 days of transport from their emission area, only 10% to 30% of the aerosol consisted of secondary and transformed aerosols. In spite of a high production during process of nucleation, the secondary aerosols advected above the Pacific Ocean will have, according to these authors, a weak impact in term of indirect radiative effect and a negligible direct effect in comparison to those of primary aerosols and species which condense onto them. In the report on the intercomparison exercise of simulation of the sulphur cycles entitled COSAM and implying 11 global models, Roelofs et al. (2001) estimate that, in winter, SO_2 oxidation in gas phase by radical OH would represent a chemical sink of about 10%, a rate which may increase up to 20% over the summer period (with a 35–45% relative uncertainty between models). Oxidation in aqueous phase would remove 42% of SO_2 over one year for the whole concerned areas, with an uncertainty between the models varying from 25 to 65%. These figures raise interrogations on the accuracy of

the assessments of quantities of sulphur compounds deposit (Roelofs et al., 2001).

In our simulations, we will take into account the BC like a single scalar, without spectral distribution in size or mass, precribed according to a constant flow in the first level of the model, i.e. diluted on the first hundred meters above surface. Once these carbonaceous soots in suspension, unlike SO_2, we do not consider a capture by mineral dust. The BC particles will thus play the role of a chemically inert tracer compared to the other pollutants. Its sinks will be managed like in the case of sulphur compounds (Fig. 3). Uno et al. (2003) modelled the BC distribution during spring 2001 over a geographical area including China, Korea and Japan, in order to retrieve the transport of these pollutants such as they were observed during the ACE-ASIA experiment. These authors coupled their chemical model CFORS with the RAMS model. They supposed that the BC particles existed in a single mode (fine mode) and chose to be unaware of any process of gravitational or wet deposit like any process of chemical conversions. They simply took account of a turbulent deposit on the surface. We followed the same assumptions in this work. Uno et al. (2003) gave a turbulent velocity for BC deposit of $1\,mm\,s^{-1}$ to the ground surface and $0.1\,mm\,s^{-1}$ on the surface of the oceans. According to previous sensitivity tests, we choose a single turbulent deposit velocity of $2\,mm\,s^{-1}$.

2.4.3 Sulphur mixing with dust

Both chemistry sulphur products and mineral dust are modified by their mixing. For example, Ma et al. (2004) established – from measurements made on the Island of Cheju, South Korea – that approximately 21% of $CaCO_3$ present in the desert mineral particles were converted into $CaSO_4$ by chemical reaction with sulphuric acid H_2SO_4 during the transport of the two mixed species. In the same way, the physico-chemical analysis of collected samples at Qingdao in October 1996 indicated that 3.3–12.2% of dust particles contained sulphates ions (and 6.5–10% of nitrates) on their surface (Zhang, 2003).

We seek here to account for the SO_2 gas capture by the mineral particles over geo-

ACPD
7, 11895–11971, 2007

graphical areas polluted by the anthropogenic emissions. The term of "capture" will be understood as an internal mixing between the two species, whatever the mechanism we did not consider BC capture or secondary sulphates capture by dust. Moreover, as explained above, $SO_2 \rightarrow SO_4^{2-}$ conversion at dust surface is not modelled, but this phenomenon can be reasonably supposed to occur quickly. The dry and wet eliminations of sulphate captured on dust particles are driven in the same manner as dust particles, i.e. gravitational dry deposition and wet removal (Sect. 2.2).

3 Orders of magnitudes of anthropogenic pollution events

3.1 SO_2 concentrations

Validation of simulations of the sulphur compounds in China can be made problematic by lack of experimental data: which orders of magnitude may be realistic with regard to the SO_2 concentrations in East Asia? In their medical study of the mortal effects of pollution by SO_2 with Beijing, Xu et al. (1994) recall that instantaneous intra urban extreme values of 630 $\mu g\,m^{-3}$ were reached in 1989, with an annual average of 102 $\mu g\,m^{-3}$. This urban annual average of approximately 100 $\mu g\ m^{-3}$ corresponds to the governmental indicators of the SEPA (State Environmental Protection Agency). At Lanzhou, a very polluted 1.5 M inhabitants city on Huanghe River (inner Mongolia), spring SO_2 concentrations are usually found between 30 and 140 $\mu g\,m^{-3}$ (Ta et al., 2004). Prof. Z. Han team gives on line the principal results of its model RAQM applied to the simulation of the sulphur and nitrated pollutants to the China-Korea-Japan zone (http://www.iiasa.ac.at/rains/meetings/6thMICS-Asia/papers/han.doc). During March 2001 and 2002, the mean concentration of SO_2 around Beijing ranged between 25 and more than 50 ppb (volume ratio, that is approximatly between 60 and more than 120 $\mu g\,m^{-3}$) while Tokyo was surrounded by concentrations exceding 200 ppb (more than 500 $\mu g\,m^{-3}$).

3.2 Sulphate concentrations

We also recall some orders of magnitude of sulphate concentrations, SO_4^{2-}. In their study devoted to the ionic composition of the $PM_{2.5}$ in Beijing, Yao et al. (2002) propose two principal production modes of sulphates: (i) gaseous phase oxidation of SO_2 in winter, (ii) an internal cloud process in summer, fast because of the aqueous phase which supports and accelerates this oxidation. Yao et al. (2002, 2003) detailed the mechanisms of formation of the secondary sulphur aerosol around Shangaï and Beijing. At Beijing, the concentration in SO_4^{2-} during spring is around the annual average concentration, say 17–18 $\mu g\,m^{-3}$. Finally, as regards Beijing, Zhang et al. (2004b) data illustrate the extreme variability of the sulphate concentrations linked to the diurnal photochemical effects and the conditions of precipitations. The concentrations in 2000 are spread around an average value of 20 $\mu g\,m^{-3}$ in May, a value appreciably lower than the simulations results of Han et al. (2004) for SO_2.

3.3 BC concentrations

BC particles originate from combustions of various types. They are seldom insulated in troposphere, because we also find Organic Carbons (OC) particles and WSOC (Water Soluble Organic Carbon). Here, we focus on BC as an anthropogenic pollution marker.

By lack of measurements of BC, the TC (Total Carbon, i.e. the sum of the various compounds) data, when available, may be considered as an upper limit for BC. The airborne measurements carried out by Huebert et al. (2004) give an idea of the TC concentrations on the Chinese coasts of the Yellow Sea and on the Sea of Japan. These measurements indicate TC concentrations higher in the atmospheric boundary layer (7.6 $\mu g\ m^{-3}$ on average) than those obtained in the free troposphere (3.1 $\mu g\ m^{-3}$ on average). In continental rural zone, in Lin'an, located approximately 200 km Southwestern of Shangaï, measured TC are 24 $\mu g\ m^{-3}$ on average since mid-February to the end of April 2001 (Wang et al., 2004).

BC was measured during ACE-Asia in Hong-Kong (China), on the island of Cheju

(South Korea) and Sado Island (Japan), for 18 months. The daily median values of PM_{10} masses were respectively 33, 14 and 11 $\mu g\,m^{-3}$ and those of $PM_{2.5}$ were worth 29, 16 and 9 $\mu g\,m^{-3}$. The mean composition, in mass, on the whole $PM_{2.5}$ for the three sites contained approximately (8.4±4) % of BC, (7.7±7) % of minerals and (43±14) % of ammonium sulphates (Cohen et al., 2004). Again during ACE-Asia, Clarke et al. (2004) investigated the mixture and optical properties of the BC possibly present in mineral dust plumes. They noted that 85% of the internaly mixed BC was in the accumulation mode and that BC accounted for approximately 5 to 15% of the mass of the mixture.

For the BC particles in Beijing, Wang et al. (2005) recall that these last few years, the total yearly consumption (industrial and domestic) of coal in Beijing was close to 1500 Mt and increases at a rate of 3.8% per annum. To estimate the BC average concentrations in Beijing, at the beginning of the winter period, we can use the diurnal variations suggested by Wang et al. (2005). Pollution by BC would decrease on average during the last few years, in spite of the increasing coal consumption, which is difficult to interpret in a simple manner. Anyhow, concentrations of several tens of micrograms per cubic meter were often measured in October and November 2000. The article by Yu et al. (2005) shows that the daily variability in BC concentrations is more important in winter than in summer but the daily averages for both seasons are of the same order of magnitude.

4 Observational data

4.1 Remote sensing data

4.1.1 Satellite

The TOMS (Total Ozone Mapping Spectrometer) aerosol index charts (not shown here, http://toms.gsfc.nasa.gov/aerosols/aerosols_v8.html), indicate a dust event initiated in

the Gobi Desert at the end of April 2005. As shown by the MODIS Terra image for the morning of April 28 (Fig. 4), the effects of this rising appear like a transport of yellow dust and will be observed over Japan in early May.

4.1.2 Ground based data (AERONET, LIDAR)

In order to constrain our work, we use the AOT and the Angström Exponent (AE) provided by the spectrophotometers of the AERONET network. From 27 April to 2 May 2005, we will analyze the records at Dalanzadgad (43 N, 104 E), in Mongolia, located near the dust emissive zones. We also use, in China, measurements in Beijing (39 N, 116 E) and Liangning (41 N, 122 E), the latter also spelled Liaoyang, located approximately 500 km in North East of Beijing. Osaka (34 N, 135 E) is the only available AERONET site in Japan during all these days. The AERONET site on Gwangju_K-JIST (35 N, 126 E, also spelled Kwangju) provides measurements for South Korea. These various sites are located as shown on Fig. 5. We also locate on this map the city of Hohhot (49 N, 112 E) in China, where the results of simulations will be discussed and compared with other ground based data, such as in situ PM_{10} measurements (hereafter refered as in situ data) and LIDAR backscattering/depolarisation images managed and provided by the National Institute for Environmental Studies (NIES, Ibaraki, Japan) according the methodology of Shimizu et al. (2004).

4.2 Surface visibility, in situ concentrations and air quality index

4.2.1 Mappings of the surface visibility data

We explain here how we easely use the visibility data. We consider a very broad geographical extension, in order to have a complete panorama of the situation. We include 950 WMO (World Meteorological Organization) stations. Among those, 732 stations were retained lastly to map the visibilities isocontours. In detail, as regards the 218 stations which were not selected, 128 were suppressed because the visibilities

are not reported there or are too much spaced in time, and the other stations proposed not exploitable temperatures (to derive RH), or gave wind speeds higher than 60 m s^{-1}, suspect values that imply mistrust of the other values measured in these same places.

We trace some of the horizontal wind speed vectors measured at the stations. They indicate the ground level air mass movements, and allow us to remark the geographically heterogeneous distribution of the measurement sites.

The maps produced by this method show the isocontours connecting between them the weather stations where the local visibility falls of an equal percentage compared to the standard local maximum value of visibility set to 100%, and this for a visibility reduction of at least 50%. Isocontours are thus right centered on the zone of less visibility, i.e. the zone where dust should be dense. At the same stations, we compute the air humidity, with special emphasis for cases where it is greater than 80%: under these conditions, fog, mist or low stratus could explain the low visibility. On the other hand, a low visibility with dry air may be attributed to dust. On the Southern China-Mongolia border, the area of interest, we find no important air humidity between April 27 and 30 (Fig. 6a and Fig. 6b). The drastic zones of visibility reduction during this period are sharply confined, which can be interpreted as mineral dust events.

On 27 April, an episode is located towards (45 N, 115 E). In the beginning of 28 April, the episode is located near the Southern point of the China-Mongolia border, an area inside 40–45 N, 100–109 E (area thereafter named “zone 1”, Fig. 2). On 29 April, over Korqin and Otindaq deserts, inside the (42–47 N, 110–119 E) area, noted thereafter “zone 2”, we note a fall of visibility due to dust transportation. In the morning of 1 May (local time), the decreases in visibility are important between South Korea and the South of Japan, but the weather conditions show condensed water (in all shapes of hydrometeors), thus do not have there a merely interpretation in term of desert dust transport.

To conclude on the use of the visibility data, we note that they consolidate the first approaches by the 24 h time-step satellite images. This method has the advantage to give an idea of the geographical extension concerned by the sandstorm with a 6 h

ACPD
7, 11895–11971, 2007

time-step.

4.2.2 In situ data and API data for Hohhot and Beijing cities

We take advantage of in situ data of surface PM_{10} concentrations for the towns of Hohhot and Beijing. We focus on these places because they are representative of 2 distinct situations of aerosols mixtures. The real-time in situ concentrations were recorded by a Chinese team collaborating with the NIES team.

Hohhot (112 E, 41 N, 1100 m, 1.5 M inhabitants) is located in Inner Mongolia, North East of the loop of the Yellow River (or Huang He), approximately 450 km West of Beijing. This city is an interesting place for aerosol measurements, because it is under the influence of winds carrying dust from Gobi Deserts, from Alxa plateau (also spelled Alashan) and Mongolia. Let's draw attention to the North and Western North mountains close to the city (whereas the 2 other cardinal directions are open on plains) where shielding effect on surface dust transport, due to this relief, cannot be neglected. Our analyses with Hohhot will be interpreted as revealing case studies of aerosol mixtures close to the mineral dust sources, but keeping in mind that Hohhot can be polluted by anthropogenic emissions, partly because of heavy industries (e.g. steel-works and power station) being located in the Western side of the city.

Beijing (116 E, 39 N, 15 M inhabitants), capital city of the People's Republic of China, is located near mountains of an average altitude of 1000 to 1500 m in the West, North and North-East. At the East, the city opens on a large plain going gradually down to the Bohai Sea, maritime outlet of the Pekinese agglomeration. The high hills account for 62% of the total surface of the city with 10 400 km^2 and the plain account for 38% with 6400 km^2. We analyze the results relative to this city as being particularly representative of the conjunction of the aerosols that interest us here: mineral dust transported by the sandstorms generated in the continental deserts and the anthropogenic pollutants emitted by the city itself and the surrounding towns.

As regards a last surface available database, we will have the opportunity – for these chinese cities – to use, as an indication and without claim of exactitude, the estimates

ACPD
7, 11895–11971, 2007

EGU

of the Air Pollution Index (API) provided by the SEPA (State Environmental Protection Administration). The SEPA is in charge to build a daily follow-up of the urban air quality in 80 cities of the country (http://www.sepa.gov.cn/english/air_s.php3). This daily value gives information about the most concentrated type of pollutant of the day. On Hohhot and Beijing, during the period under study, the prevailing pollutant is always indicated as "PM_{10}" by the SEPA, which means that pollution was controlled by particulate matter: it can include mineral dust. In case of prevailing gas pollution, the API would be either SO_2 or NO_x, but that case never happened during this period.

With the help of the conversions tables of daily API into daily means PM_{10} concentrations, valid for 6 successive linear intervals limited, by construction, between a minimum of 50 $\mu g\,m^{-3}$ and a maximum 600 $\mu g\,m^{-3}$ for PM_{10}, we find, by polynomial regression, a continuous easy-to-use conversion law:

$$PM_{10}\left(\mu g\,m^{-3}\right) = 8.10^{-6}\,(API)^3 - 8,7.10^{-3}\,(API)^2 + 3,6706\,(API) - 121,27 (R^2 = 0.9968) \quad (1)$$

Some authors (Li et al., 2003; Guo J. et al., 2004; Han et al., 2004) regard – as ourselves – API as an interesting indicator of the episodes of mineral dust, like in Beijing (Zhang et al., 2003b) and use API to extrapolate the concentrations of various specific species of aerosols. As it is difficult to know what is exactly chemically meant in the "PM_{10}" mass load, and as API are only daily averages, we will not interpret them more accurately than an rough order of magnitude of the concentration in mixture of particles with diameters lower than 10 μm, as far as these particles do not exceed actually 600 $\mu g\,m^{-3}$ because the corresponding API are not defined beyond (this value of 600 $\mu g\,m^{-3}$ is a "saturation" maximum value).

ACPD
7, 11895–11971, 2007

5 Results and discussions

5.1 General overview

5.1.1 Dust flux budget

Information on dust emissions is summarized in Table 1. Dust fluxes are presented over 3 source areas (Fig. 2): zone 1 (south of Gobi desert, remote from shoreline), zone 2 (SE Gobi desert) and zone 3 (overall Gobi, which roughly covers the whole emission areas). Note that the relative anticyclonic situation over Taklamakan prevents any intense dust uptake from this desert during the period under study. Zones 1 and 2 are approximately of same size (about 440 000 km^2). We present the local maximum uptake for every 3 h-interval modelled within each zone. The detailed results (not shown) highlight the extreme variability of dust emissions, which is represented here by the standard deviations: they are of the same order of magnitude than the average value itself. Moreover, the modelled values agree with the literature data (summarized in Lasserre et al., 2005).

5.1.2 Surface plumes of dust, SO_2 and BC particles

We show the main features of dust and anthropogenic species, and we compare with observational (and literature) data, from 27 April to 2 May. Figs. 7a to f are an overview of the surface plumes at 00:00 UTC (~08:00 LT).

The anthropogenic pollutants plume is located along the shoreline from Shanghai to Koreas and Japan Sea via Beijing, which gradually extends towards Japan. During 1 May and 2 May, concentrations in SO_2 exceeding 40 $\mu g\,m^{-3}$ are modelled over the Eastern China Sea and South Japan while BC concentrations higher than 2 $\mu g\,m^{-3}$ are found. Note that the extreme SO_2 concentrations in the figures (greater than 300 $\mu g\,m^{-3}$) are just found on few places (near Shanghai or Seoul, for instance). Such values are sometimes observed in Asia (see 3.1), but are not typical features of the

ACPD
7, 11895–11971, 2007

whole area: the modelled values are generally lower than 200 $\mu g\,m^{-3}$.

The same occurs with BC, as the maximum model values are about 40~50 $\mu g\,m^{-3}$. Those maxima are consistent with literature data. Even if we exclude extreme values – for instance, 500 $\mu g\,m^{-3}$ reported at Jianxiang bridge at Beijing during winter 2000 – winter data recorded at this place range between 10 and 70 ppb, say 25 to 180 $\mu g\,m^{-3}$ (Sun et al., 2006). Farther from megalopolis, the model BC concentrations lie between 1 to 15–20 $\mu g\,m^{-3}$, also in agreement with the observations reported in literature.

The modelled surface dust plumes (Fig. 7) patterns highlight the contrasting origins between desert particles and pollutant sources, along with the particular role of wind in aeolian emission. The intermittency is therefore a common rule for desert dust, not for anthropogenic pollutants. From these figures, it appears that the mixing zones of anthropogenic and mineral pollutants are of limited extent because the anthropogenic pollutants are on the East and South-East of the modelled area when mineral dust plume lies from the centre to the East and South-East area. Until 1 May, the mineral dust plume seems to blow the anthropogenic pollutants already present in the atmosphere in front of him. This partition between natural and anthropogenic aerosols inside the boundary layer is confirmed by observations. Recent studies of particles collected at Qingdao (south of Beijing) during 3 dust storms of spring 2001 revealed that mineral aerosol compositions showed rarely indications of mixing with anthropogenic pollution (Zhang et al., 2003c) before their arrival above the metropolis, even for a long-range distance as, for instance, a transport from Northern deserts to Taiwan (Lin et al., 2007).

Behind the dust front, when the dusty air mass lies above the sources of pollution, it is permanently resupplied with the local anthropogenic pollutants which favour some vertical mixing (and SO_2 uptake onto dust particle as explained in next section). However, as a general rule, the different aerosol species are modelled in separate plumes.

Sulphate concentrations are widespread on the whole marine and coastal domain with a maximum about 5 $\mu g\,m^{-3}$ to the North of Japan since the 29 April. This agrees well with the Matsumoto et al. (2003) report who noted that pollution by the nss-SO_4^{2-} often preceded the other anthropogenic pollutants and that these species could be

ACPD
7, 11895–11971, 2007

EGU

followed by polluted mineral particles. The authors measured the average concentration of anthropogenic sulphates on Rishiri Island, North of Japan, with approximately 2.5 $\mu g\ m^{-3}$ in spring, and some higher values in the case of abrupt incoming of continental polluted air masses. This behaviour is also true over the continent itself were we find peaks of concentrations towards Shanghai and Seoul, certainly over-estimated (70–80 $\mu g\,m^{-3}$), but with a very sharp gradient around these extremely localized zones. Most situations give model concentrations lower than 30–40 $\mu g\,m^{-3}$, in agreement with the annual mean average values given by Wang et al. (2006) (ref. inc.), that is 18 $\mu g\,m^{-3}$ for Shanghai in 2003–2005, with an average during spring of 21 $\mu g\,m^{-3}$, 44 $\mu g\,m^{-3}$ at Guangzhou in 1993, 18 $\mu g\,m^{-3}$ at Xiamen in 1993, 22 $\mu g\,m^{-3}$ at Guiyang in 2003 and 12 $\mu g\,m^{-3}$ at Dalian city during 1994–1995. We did not examine in detail the role of liquid water (wet scavenging). It is however certain that water was involved in the capture of the pollutants. This point will be addressed in later studies, with the help of chemical data concerning the wet deposits.

In conclusion of our simulation of horizontal transport of the four species of pollutants, we show that the mixings of desert dust plumes with the pollutants in East Asia seem to follow a spatially inhomogeneous process. As Zhang et al. (2005) record it at Qingdao in February and March 2002, mineral dust coming from the north of the country seems to be confined during several days in the post-frontal air mass whereas the anthropogenic pollutants are found in the pre-frontal boundary layer. The mixing – mineral/pollution - can take place within the interface of these air masses or through a slow diffusion process in a calmer air, as it seems to happen on 2 May.

5.1.3 Captures of SO_2 by mineral dust

Figures 8a and b give respectively horizontal (near surface) and vertical zonal cross-section modelled dust plumes, along with SO_2 captured by dust, at 00:00 UTC (08:00 LT) on 1 May. The area of captured SO_2 extends to the South and the East and follows the front of the mineral plume. On 28 April 00:00 UTC (not shown) desert dust just arrives in the zone already polluted by SO_2 over the Bohai Sea. We find a

maximum of 11 $\mu g\,m^{-3}$ in SO_2 captured by dust at surface level, and this value will increase during the following days. On 29 April, both dust and free SO_2 surface plumes are more mixed and the overlapping zone shows a 13 $\mu g\,m^{-3}$ maximum of captured SO_2 above the Bohai Sea. We find 44 $\mu g\,m^{-3}$ on the West shore of South Korea while it is less than 4.4 $\mu g\,m^{-3}$ over the Japan Sea, where, at the same time, "clean" mineral dust concentration does not exceed 200 $\mu g\,m^{-3}$. The simulation showed a notable dust emission starting from the end of 30 April. On 1 May (Fig. 8a), as the horizontal gradients of surface concentration at the Southern and East dust front are very important, the mixture only takes place inside a bow-shaped area of approximately 200 km in depth. On 2 May, wind intensity decreases in the South and dust spreads over the most polluted zone, so that an increasing fraction of SO_2 is captured by mineral particles. Maximum surface values from South to North of China Sea shoreline vary from 93 $\mu g\,m^{-3}$ (Shangaï) to 41 $\mu g\,m^{-3}$ (West of South Korea).

We display on Fig. 8b a vertical zonal cross-section of the plumes sufficiently at the North of the simulated zone (pink line, Fig. 8a) so that the modelled vertical profiles are representative of transport likely to pollute Japan and illustrate a regional situation of quasi permanent pollution. Figure 8b superimposes the SO_2 concentrations captured by the mineral dust and isolines of mineral dust concentrations itselves. The 3-h sequence shows that, after the westerly dust front income, the mixing between SO_2 and mineral plumes (delineated by the minimum 50 $\mu g\,m^{-3}$ red isoline), always occurs between surface and 2000 m a.g.l. on 29 April and 30 April, and until approximately 4000 m on 1 May, with, at these altitudes, values of captured SO_2 concentrations about 0.1 $\mu g\,m^{-3}$. The captured SO_2 concentrations decrease very quickly with altitude, and more quickly, as a whole, than the concentrations of dust and free SO_2 do. In the lower layers, the maxima of captured SO_2 concentrations are found especially from North of the Bohai Sea to Japan. Over the Sea of Japan, the calculated surface concentrations are lower than 7 $\mu g\,m^{-3}$. The maxima in the whole of the vertical section are (every day at 00:00 UTC) as follows: 7.2 $\mu g\,m^{-3}$ for 28 April, 4.3 $\mu g\,m^{-3}$ for 29 April, 4.3 $\mu g\,m^{-3}$ for 30 April, 4.8 $\mu g\,m^{-3}$ for 1 May and 9.1 $\mu g\,m^{-3}$ for 2 May, 2005.

ACPD
7, 11895–11971, 2007

EGU

In order to qualitatively illustrate the spatio-temporal capture mechanism, Fig. 9 displays the chronological evolution of the vertical distribution of SO_2 captured by dust above Beijing. The captured SO_2 concentrations (symbolized by full circular surfaces, with size proportional to captured SO_2) lie between 10^{-3} and $0.5\,\mu g\,m^{-3}$ (magnitudes are specified in some points). This figure gives an idea of the relative intensities of the captures in time and altitude.

It is interesting to note that on April 28, when dust surface concentrations increase, the capture of SO_2 does not increase immediately and exhibits a rather homogeneous vertical profile between 100 m and 1000 m. The highest concentrations, located under 2000 m a.g.l., are found in the hours thet follow the dust surface maximum of 28 April. The mixing process occurs in a deepening layer, which reaches 4000–5000 m on late 29 April (UTC). From 30 April, the mixing process interrupts by lack of dust.

5.2 Model concentrations and validations of mineral dust over Hohhot and Beijing

Hourly meteorological data are available on the general public site http://www.wunderground.com. For Hohhot, during local April 27 afternoon, South-Westerly wind blew between 3 to $14\,m\,s^{-1}$ in gusts and turned North from 23:00 LT with a visibility falling to 3 km before rising to 7 km after midnight (see http://www.wunderground.com/history/airport/ZBHH/2005/4/27/DailyHistory.html). From midnight to 07:00 LT on 28 April, the recorded visibility ranged between 300 and 1000 m under Northern and North-Westerly winds of 3 to $7\,m\,s^{-1}$. This first dataset confirms the occurrence of a dust plume over Hohhot coming from North.

5.2.1 Hohhot dust surface concentrations

We present the time serie of the surface mineral dust concentrations, on Fig. 10, modelled at Hohhot city. We superimpose the in situ recorded concentrations and the daily PM_{10} concentrations deduced from the API data. On the same figure, as further discussed, we also display the modelled mineral dust column load over Hohhot.

An intense dust episod is clearly identified in the morning of 28 April in local time (end of 27 April, UTC). The time serie of surface concentrations for 27 and 28 April presents a phase delay of a few hours as compared to the column loads. Thus, the model calculates a transport of dust occurring in a differentiated way according to altitude. The maximum surface concentration modelled for 30 April is synchronized with those of the dust column loads: this second dust front was close to the surface. Modelled dust concentrations agree with in situ data and API data for the main tendencies but some discrepancies are found. The correlation coefficient between in situ data and model products is 0.49 which is significant with a real-time simulation using a 3 h output frequency. Model results underestimate the observations for the main event of 28 April, which was prolonged until 29 April, according to local measurements. The PM_{10} values from API of 28 and 29 April approach the possible maximum values for the API indices. These PM_{10} values must thus be considered as estimates of the lower limits of the actual average concentrations for these two days. For the second dust event, on 30 April, we note, contrary to the previous days, a model overestimation as compared to in situ measurements, but a very good agreement with the estimate of the interpolated PM_{10}. Eventually, all the 3 sets of values (calculations of the model, in situ measurements and PM_{10} deduced from API) closely converge at the beginning of May, showing, with values of about $100\,\mu g\,m^{-3}$, a reduction in surface dust transport.

Calculations of concentrations in Hohhot are certainly not perfect if compared with in situ measurements, but they rather accurately transcribe the chronology and the global evolution of the amplitude of these surface measurements. Thus, we now examine how the model simulates the vertical profile of transport of dust over Hohhot.

5.2.2 Hohhot dust vertical profiles

Figure 11a shows the vertical profiles of mineral dust concentrations every 6 h, on the first 4500 m a.g.l. (16 first levels RAMS) above Hohhot. The modelled profile on 27 April at 12:00 UTC shows a maximum concentration of approximately $600\,\mu g\,m^{-3}$ around 1000 m, which corroborates the assumption of a sandstorm having flown over

Hohhot in altitude before the dust transported to the surface does arrive on the city itself (which is probably an orography effect). At the end of 27 April, the simulated ground concentration is twice less than the 1000 m value. Six hours later, the profile shows an inversion of tendency near ground and this is completely marked on 28 April at 00:00 UTC where the concentrations decrease in a quasi-monotonous way with altitude (about 700 $\mu g\,m^{-3}$ at surface level and near 170 $\mu g\,m^{-3}$ at 1000 m). On 30 April, at 00:00 UTC (08:00 LT), the second dust event is initially close to the ground, then the profile bends and a maximum appears between 1000 m and 2000 m 12 h later. As this event comes from North, we again hypothesize effects of relief in the abrupt variations in the shapes of the dust vertical profile.

Figure 12a shows the LIDAR normalised Backscattering Intensities (hereafter referred to as BI) and Depolarization Ratios (DR) at 532 nm wavelength for the first 3000 m over Hohhot area from 27 April at 06:00 UTC, the atmosphere contains no depolarizing aerosols, i.e. mainly anthropogenic pollutants. The first event (27 April) exhibits a vertical extension higher than 2000 m, similar to model results (with a few hours of delay). Then, LIDAR products show a transition with "mixed" aerosols, with a vertical extension exceeding 2500 m a.g.l. Just after 12:00 UTC, also on 27 April, LIDAR data show a brutal decrease in the BI level, that limits to the first hundreds meters: it indicates an aerosol plume at very low altitude, while the DR abruptly increases and reaches more than 30% between the ground and 1000 m, strongly suggesting that there are mineral aerosols (depolarizing particles) brought by the sandstorm. On 29 April, we note a reduction in the BI and DR as well, indicating a less polluted day. On 30 April, around 00:00 UTC, the DR increase suggests a new arrival of mineral particles, also retrieved by the model. It is more difficult to interpret the form of this LIDAR observation, but it exhibits a vertical extension again exceeding 2000 m, which corroborates our profiles calculations around 30 April at 12:00 UTC (Fig. 11a).

As a whole, our simulations at Hohhot roughly agree with the overall evolution of the LIDAR backscattering shape.

ACPD
7, 11895–11971, 2007

5.2.3 Beijing dust surface concentrations

Two sandstorm events occurred between 27 April and 2 May 2005 over Beijing. The first one (27 and 28 April), is related to the intense dust transport already mentioned at Hohhot (see above) for the same dates. The second episode was observed at Beijing rather than Hohhot. Figure 10b presents the time series of the simulated surface concentrations as well as the estimates of the daily averages of the PM_{10} concentrations derived from the API.

For the first dust event, in situ measurement at 21:00 UTC on 27 April (i.e. approximately 05:00 LT, 28 April in the morning) is 510 $\mu g\,m^{-3}$, which closely agrees with model values: modelled maximum ground concentrations range from 570 to 620 $\mu g\,m^{-3}$. For 28 April, the average PM_{10} from API is estimated at 480 $\mu g\,m^{-3}$. The duration of the episode is approximately 9–12 h according to our calculations, which correctly contain the peak of in situ measurements.

After this dust event and until 30 April, Beijing is not concerned by substantial dust transport, but always remains with a non negligible background pollution content (see on 29 April: in situ data are often higher than 200 $\mu g\,m^{-3}$ and PM_{10} from API reach 160 $\mu g\,m^{-3}$). Model results (i.e. desert dust component) present a rather satisfactory order of magnitude. The second dust event (30 April and 1 May) is also retrieved by the model, with similar orders of magnitude in dust concentrations (200–400 $\mu g\,m^{-3}$), in spite of some temporal model delay.

In Beijing, the overall correlation coefficient between the results of 3 h real-time modelled surface concentrations and in situ measurements is 0.56.

5.2.4 Beijing dust vertical profiles

The column loads in mineral dust are also shown on Fig. 10b. The phase coincidence of the two curves – ground concentrations data and column load – suggests that the dust events on Beijing were relatively homogeneous with altitude. According to the curves of Fig. 11b, on 27 April, between 00:00 and 06:00 UTC, dust looks very homo-

ACPD
7, 11895–11971, 2007

EGU

geneous in the vertical (concentration varies slowly from the ground to approximately 2500 m) ranging from 180 $\mu g\,m^{-3}$ to about 100 $\mu g\,m^{-3}$. This first event is forerunner of the most intense phenomenon that occurs 12 h later approximately, after a transition with a less polluted air. More complex profiles showing high values in altitude (550 $\mu g\,m^{-3}$ around 2000 m on 27 April, 18:00 UTC) are following. Initially in "shark nose" (18:00 UTC), the vertical dust profile evolves to form two layers: a first one near surface (maximum around 620 $\mu g\,m^{-3}$), and a second one between 2000 and 2500 m a.g.l., where the concentrations exceed 200 $\mu g\,m^{-3}$, on 28 April, 00:00 UTC. Lastly, the profile of the episode of 30 April looks like what was simulated on 27 April, i.e. a rather homogeneous profile with concentrations higher than 200 $\mu g\,m^{-3}$ on the first 2000 m a.g.l.

We present on Fig. 12b the LIDAR measurements (BI and DR) recorded at Beijing at the end of April 2005. Now, we compare these data to our simulations of dust vertical profiles. We find the confirmation of a relatively homogeneous vertical distribution between surface and 1500 m for the arrival of the 27. The intermediate DR (~10%–20%) is the signature of a mixing of anthropogenic and dust aerosols. From April 27, 18:00 UTC, i.e. early local morning of 28 April, the BI grows suddenly, showing the arrival of the dust plume, initially near surface (maximum height ranging between 500 and 1000 m) as we calculated for 28 April, 00:00 UTC. During the day, the LIDAR patterns (BI) exhibit stratification around two layers (0–1000 m and 2000–3000 m) whereas the DR strongly suggest a complex mixing of the aerosols shapes. The second event (on 30 April, between 0 and 12:00 UTC) appears localized lower than 1500 m a.g.l. The DR shows that this last event carries a load in mineral aerosols lower than the event of 28 April.

To conclude this part devoted to the results of real-time modelling from transport of mineral dust over Beijing, we estimate that they suitably represent the qualitative and even quantitative aspects of the event that really occurred.

ACPD
7, 11895–11971, 2007

5.3 Modelled anthropogenic pollutants (BC, SO_2 and SO_4^{2-}) on Hohhot and Beijing

We now describe the modelled surface concentrations of the anthropogenic pollutants: BC, SO_2 and sulphates. We adopt a presentation by pollution species at the same dates in Hohhot and Beijing: BC on Fig. 13a, SO_2 on Fig. 13b and sulphates on Fig. 13c. We also show on these figures the respective column loads, which will be further useful for the calculations of the optical thicknesses. Lastly, Table 2 summarizes some statistics of the representative values for all of the five simulated days, from 27 April (00:00 UTC) to 2 May (00:00 UTC) 2005.

5.3.1 Time series of the BC surface concentration and column load at Hohhot and Beijing

We see in Beijing (Fig. 13a) a daily modulation of the BC contents whereas the BC variations in Hohhot do not exhibit such a daily variability (which could be explained by contrasting stability diurnal patterns). During the surface concentration oscillations, from 28 to 30 April in local time, BC pollution continuously increases at the vertical of Beijing. This BC contribution, in altitude, could originate from the polluted zones of the coastal urban sources, according to the winds coming from South-eastern areas from 14:00 LT, 28 April to 04:00 LT, 29 April, and turning to Northern wind during five hours before coming again from the South-East for the rest of the day (see http://www.wunderground.com/history/station/54511/2005/4/30/DailyHistory.html).

At the end of the simulated period, on 2 May in the morning, we model an intrusion of BC pollution in Hohhot. That seems compatible with the local wind observations, which came from the East and the South East (thus from the polluted zones closer to the coast) from 20:00 LT the day before, at the evening. BC concentrations are logically higher in Beijing than in Hohhot, but it does not appear an obvious correlation of the BC pollution events over these two cities.

ACPD
7, 11895–11971, 2007

5.3.2 Time series of the SO_2 surface concentration and column load at Hohhot and Beijing

First of all, it will be noticed (Fig. 13b) that SO_2 concentrations follow variations very close to those of BC. That is explained, on the one hand, by the common mode of injection for these two pollutants in the model, and, on the other hand, by the geographical proximity of their emitting zones. The few differences of surface concentrations curves will thus be explained primarily by the very local differences in the atmospherical dynamics, throughout their respective ways (there is of course not an exact proportionality between the BC and SO_2 fluxes in each source pixel), like by the specific (model) behaviour of SO_2.

Modelled SO_2 values (see Table 2) appear completely relevant in China, in Beijing like Hohhot, due to the presence of factories. Literature gives SO_2 orders of magnitude of several tens of $\mu g\,m^{-3}$. For example, Zhang et al. (2005) report, during March 2000, SO_2 concentrations ranging between 35 and 70 ppb (approximately 90 and 180 $\mu g\,m^{-3}$) in a polluted air just before a sandstorm front. SO_2 concentrations ranged between 10 and 60 ppb (approximately 25 and 150 $\mu g\,m^{-3}$) during the 24 h that followed the mineral dust event. In the rural area of Lin'an, 200 km West of Shanghai, time average of SO_2 concentration (established from mid-February to the end of April 2001) is 15.9±14.6 ppb (Wang et al., 2004), which means that, approximately at 200 km of an urban megalopolis, SO_2 concentrations are characteristic of a rather clean air with maximum peaks of pollution around 30 ppb, say 75 $\mu g\,m^{-3}$. According to the same authors, the daily averages of SO_2 measured in downtown Beijing in April 2000 reach 60 $\mu g\,m^{-3}$ in little dust periods and are about 19–24 $\mu g\,m^{-3}$ during two monitored dust plumes.

Satellite SCIAMACHY data (not shown) reveals the presence of SO_2 over the South Beijing and the Bohai Sea on 29 April 2005. Recall that above Bohai Sea, the daily SO_2 concentration may exhibit a strong variability: airborne measurements (400 m to 800 m a.s.l.) in March 2002 found that SO_2 ranged between 20 and 40 ppb, i.e. roughly

ACPD
7, 11895–11971, 2007

EGU

50 to 100 $\mu g\,m^{-3}$ (Hatakeyama et al., 2005).

During the period under study, we had no measurements in Beijing, but it has been possible to directly compare our model results with observation data from API measured at Tianjin (http://www.tjemc.org.cn), which is fairly representative of the Beijing area. Precisely, Tianjin city (117 E, 39 N) is located at the Western point of the Bohai Sea and approximately 150 km South-East of Beijing. Here, API data does not refer to PM_{10} aerosols (Sect. 4.2.2): in Tianjin, the API index specifically refers to SO_2 (as this pollutant was predominant). On 30 April, the local SO_2 estimates from API give a concentration of 111 $\mu g\,m^{-3}$, which compares with the model SO_2 results: 171±137 $\mu g\,m^{-3}$ (average ± standard deviation). On 1 May 2005, the SO_2-API index gives a concentration of about 60 $\mu g\,m^{-3}$, and the model calculates a SO_2 concentration of 65±43 $\mu g\,m^{-3}$. The model results in Tianjin thus seem to reflect in a correct way the reality of local SO_2 pollution during these two days.

We will discuss the vertical column load of SO_2 pollution as shown on Fig. 13b to compare it with the sulphate ones

5.3.3 Time series of the SO_4^{2-} surface concentration and column load at Hohhot and Beijing

The sulphate ions SO_4^{2-} are secondary pollutants resulting - in our simulation – from SO_2oxidation. The SO_4^{2-} columnar load bars (Fig. 13c), for both cities, closely follow the SO_2 bars and represent between the third and half of SO_2 loads. As regards surface concentrations, both Figs. 13b and c show, over Beijing, a very emitting zone of pollutants, a marked temporal modulation in SO_2, whereas the SO_4^{2-} looks much smoothed in time.

In this study, we do not have any sulphate observational control values, so that we must limit to compare model results with literature data. Actually, sulphate concentrations are very dependent on the temperature and local RH: for instance, important relative moisture accelerates the $SO_2 \rightarrow SO_4^{2-}$ conversion, which would, otherwise, fol-

low a dry process (the only process taken into account in the model). This was shown in Beijing by Yao et al. (2003): according to these authors, sulphate concentration is higher in summer than in spring because of intra cloudy processes and higher temperature. So, they found summer concentration in secondary sulphates of 31.5 $\mu g\,m^{-3}$, which gives us an upper order of magnitude for Beijing. On 29 April 2005, the weather was rather clear in Beijing with low relative moisture (35% on average). We simulate, for the following 24 h, a rise of the SO_4^{2-} content from 4 to 17 $\mu g\,m^{-3}$. Our estimate, under conditions probably favourable to a dry conversion, thus agrees with Yao et al. (2003) orders of magnitude and consolidates the credibility of our results for the SO_4^{2-} concentrations.

5.4 Optical signatures

5.4.1 Principles for the calculation of the Aerosol Optical Thickness

The simplified representation of the aerosols cycle taken into account in this study must find a validation in physical measurements also easily accessible. As stated above, we chose to compare our results with the radiometric data: Aerosol Optical Thicknesses τ (AOT) and Angström Exponent α (AE), both characteristic of the aerosols present in the atmosphere.

In order to estimate the observed AOT, we adopt the following simplification: each of the four types of studied aerosols (mineral dust, BC, free SO_4^{2-} and SO_4^{2-} on dust issued from oxidation of the captured SO_2) is allotted a specific extinction section $\sigma_{j\text{ext}}$, in $m^2\ g^{-1}$. The specific extinction section $\sigma_{j\text{ext}}$ cumulates, in a single physical variable, the specific aptitudes of the aerosol to absorb and scatter the solar radiation in the UV, visible and IR wavelengths. The essential interest of $\sigma_{j\text{ext}}$ consists in its easy-way to use, because it just needs to be multiplied by the vertical column load C_j(in $g\,m^{-2}$) of aerosol species j, to directly obtain the specific AOT for this aerosol

$$\tau_j = \sigma_{j\text{ext}} C_j \quad (2)$$

Of course, this simplification is carried out to the detriment of a rigorous determination of $\sigma_{j\text{ext}}$ because, as e.g. explained by D'Almeida et al. (1991) or Seinfeld and Pandis (1998), this coefficient depends, in the low atmospheric layers, not only on the chemical nature of the aerosol but also, amongst other, on the wavelength (see also Fialho et al., 2005), on its real shape (granulometry size distributions, Chin et al., 2002; Kalashnikova and Sokolik, 2002, and individual forms, Kasparian, 1997), and on how it can be agglomerated with other species in aqueous or solid phase (Martins et al., 1998; Ricard, 2001). Note that the sulphates have a diffusivity quickly increasing with RH (Lowenthal et al., 1995; Carrico et al., 2003) and that, if the sulphates are coated on a BC nucleus, the absorbing capacity of BC increases by a factor of 2 to 2.5 as compared with BC alone (Sato et al., 2003). These remarks explain why the observed values of the extinction coefficients are highly scattered: Table 3 gives the bibliographical values of cross sections of extinctions (majority established between 500 and 600 nm and for various moistures). We based upon this table to make our choice of representative values of σ_{ext} for the four aerosols. As regards SO_2 captured by mineral dust, we no longer consider it as a gas, but as an aerosol, because, as explained above, we assume that it is quickly transformed into sulphate: we allot it with a $\sigma_{\text{sulphate}/d\text{ext}}$ value equal to the free sulphates.

The σ_{ext} values were ruled as:

Sulphates: σ_{SO4ext}=8 $\text{m}^2\,\text{g}^{-1}$; Black Carbon: $\sigma_{BC\text{ext}}$=12 $\text{m}^2\,\text{g}^{-1}$;

Mineral dust: $\sigma_{d\text{ext}}$=1.2 $\text{m}^2\,\text{g}^{-1}$; Sulphates on mineral dust: $\sigma_{\text{sulphate}/d\text{ext}}$=8 $\text{m}^2\,\text{g}^{-1}$.

5.4.2 Validation of modelled AOT with the AERONET AOT and AE data

We display every 3 h, from 27 April to 2 May 2005 at 00:00 UTC, the AOT of the atmospheric columns according to the simple formula:

$$\tau = \sum_{j=1}^{4} \sigma_{j\text{ext}} C_j \qquad (3)$$

ACPD
7, 11895–11971, 2007

EGU

We also model, inside the total AOT, the partition of the AOT related to each of the four aerosol species in order to estimate which one dominates the extinction of the solar radiation. Lastly, these modelled AOT are validated by comparison with the time series of the AOT and the AE data provided by the AERONET network of photometers, at five locations: Beijing, Dalanzadgad, Liangning, Gwangju and Osaka.

A study distinguishing four aerosols (mineral, sea salts, SO_4^{2-} and BC) was carried out in order to compare model results and measurements (Takemura et al., 2003). In their study, the calculations concern the daily averages of the radiative effects over the East-Asian Seas and the Northern Pacific. At larger scales, comparison between model and data from photometers and satellites were also used to quantify the total radiative impact over the Northern hemisphere, of the East-Asian aerosols produced in spring 2001 (Chin et al., 2004). On the other hand, our aim was not to compare average optical thicknesses with broad temporal and large space scales, but to directly confront the 3 h – real time model output with the instant data at each measurement site (Fig. 5): Dalanzadgad (Mongolia), Beijing, Liangning (NE China), Gwangju (South Korea) and Osaka (Japan).

The AERONET AOT data are of three quality levels: 1.0, 1.5 and 2.0. Although it is recommended to publish results based on the level 2.0 values (Eck et al., 2005, and personal communication), we knowingly took the party (and risks too) to directly use the "rough" data of AOT of level 1.0 because postprocessings of levels 1.5 and 2.0 tend to smooth the time variations of the AOT by removing certain high values (which could be due to clouds, but also to thick dust plumes). These levels prevent, in turn, from well taking into account, "in real time", of the transport of the Asian aerosols.

For clarity, we only use the AOT at 500 nm (Dalanzadgad, Liangning) or 675 nm (Beijing, Gwangju, Osaka) at each time step. However, in order to bring more information about the nature of the aerosol via its spectral signature, we also plot the AE, defined by Angström (1964):

$$\alpha = \ln\left(\frac{\tau_{\lambda_1}}{\tau_{\lambda_2}}\right) \Big/ \ln\left(\frac{\lambda_2}{\lambda_1}\right) \quad (4)$$

ACPD
7, 11895–11971, 2007

EGU

where τ_{λ_1} (resp. τ_{λ_2}) is the AOT corresponding to the wavelength λ_1 (resp. λ_2). We used AE data with λ_1=500 nm and λ_2=870 nm.

When α ends towards zero, the size of the aerosols is often in the accumulation or the coarse mode. Otherwise, when α increases, say of the order of 1, the size of the aerosols tends towards very fine modes, even molecular dimensions. Generally, AERONET provides AE (α) ranging from 0 (or even slightly negative) to 0.7–0.9 for mineral particles, from the desert zones to the area where they first mix with other aerosols, and in an interval from 1.2 to 2.5 for urban pollution aerosols (Dubovik et al., 2002; Smirnov et al., 2002). When mixing is present, intermediate values may be found: for example, a value of α=0.95–1.02 was measured in December 2000 by Sano et al. (2003) at Amami-Oshima island (Southern Japan), indicating a mixing of small and large particles; in the same experiment, these authors found a lower average of 0.66 when the desert dust ratio was increased.

(i) Beijing

Figure 14a shows the time series of modelled AOT over Beijing and the corresponding AOT and AE (α) AERONET data.

The AOT, for five days, is modelled as τ_{Beijing}=0.74±0.36 (average ± standard deviation), with a minimum at 0.22 before the first dust event, and a maximum at 1.99 on 27 April, 18:00 UTC (02:00 LT, 28 April) during the desert dust storm. In rather comparable conditions, during spring 2001, Xia et al. (2005) found a mean AOT (500 nm) ranging between 0.68±0.06 and 0.81±0.70. We are not far from this magnitude. Finally, our results agree very well with the monthly mean of about 0.6 for April-May recorded by Qiu and Yang (2000) from 1980 to 1994.

AERONET data are diurnal observations, so note that we have constraint points only during approximately half of the studied days. However, the observed shape during the local day (since 00:00 UTC to 12:00 UTC roughly) is roughly retrieved, day after day, by the model AOT. The observed and modelled values of April 28 and 30 are in agreement in the evening. Moreover, the model AOT lower than 0.6, before and after

the dust events, agree very well with data of Beijing, but AERONET data for the 29 April are higher than our calculations.

The AE observed in Beijing suggest that the hourly contribution calculated for each aerosol is relevant. In the hours before the first sandstorm, the AOT between 0.2 and 0.6 show a composition of an air rather little polluted, and the AE values (around 0.5) suggest that this pollution is an anthropogenic and mineral mixing, but dominated by mineral. 24 h later, the AE are weak or even negative: the aerosol dominates in the coarse mode, which is a proof of the mineral plume, as simulated by the modelled partition of the AOT peak. On 29 April, and even more on 30 April, the increase in modelled anthropogenic contributions is clear and is underlined by the significant increase of the AE data. Lastly, after the second dust plume, on 1 May, we find the optical characteristics of a mixed aerosol (α ranging between –0.2 and 0.5).

In conclusion, our simplified restitution of the optical characterization of the cycle of the natural and anthropogenic aerosols over Beijing seems to be relevant.

(ii) Dalanzadgad

This AERONET site is located South of Mongolia, close to the emitting dust deserts. It is thus unsurprising to model AOT values with a major part of dust contribution (Fig. 14b).

Our AOT estimates correctly agree with the observed tendencies for the first dust event of 27–28 April. On 28 April, the low AE values ($\alpha \sim 0$) confirm the mineral prominence within the aerosol plume. On the other hand, we underestimate the dust quantity itself because the observed AOT are twice more important than the modelled AOT, with some hours in advance.

About the real-time discrepancies, we think that the short distance between the desert source and the AERONET site must be seen as the main cause of the delay between the extremes of observed and modelled AOT. The measurement site can detect some much localized epiphenomena that our spatio-temporal resolution cannot take it into account.

ACPD
7, 11895–11971, 2007

EGU

We correctly model a dust plume, over Dalanzadgad area, during 29 April. For the following days, we also correctly retrieve the quick variations of AOT, but smoothed in time, with a dominant presence of mineral dust.

(iii) Liangning

Liangning, a Chinese city located on the North shore of the Bohai Sea, is polluted by local anthropogenic emissions, and by mineral dust coming from the close East Gobi deserts (Horqin, Otindag and Hulun Buir as well). Figure 14c shows, for 27 and 28 April, some modelled AOT with an opposite tendency compared to the few data we can compare. AE data suggest a mineral mixed aerosol. We probably underestimate a dust plume crossing over Liangning during 27 April, a hypothesis sustained by the MODIS imagery but not confirmed by the TOMS Aerosol Index for that day. Another possibility is that the model drives the dust plume too much Northerly than it actually was, so that we miss Liangning. The last hypothesis is that the few level 1.0 data are inappropriate because of clouds, which would be a limit for our methodology.

The days of 29 and 30 April are, on the contrary, much better described by the AERONET data. We can see that the modelled AOT follow the observed tendency, concerning the time series and the order of magnitude itself. We probably underestimate the mineral load carried to Liangning on 30 April, as the model reaches half of the observed AOT peak at the same time. This model delay explains why, in opposite way, we overestimate the AOT 24 h later with a major mineral composition whereas the AE (α) suggest finer aerosol inside the plume. The model estimates a major arrival of sulphates on 30 April but we can not discuss further this relative contribution to the total AOT because, as we said above, we underestimate the mineral contribution on the same time.

To sum up the Liangning case, the model AOT ranges between 0.07 and 2.01 (in average $\tau_{\text{Liangning}}$=0.84±0.56) and agree with the mean orders of AOT observed over the five days. In magnitudes, for example, Xia et al. (2005) give an average AOT of 0.60±0.40 for spring 2001 over Shenyang city located 100 km NE of Liangning.

ACPD
7, 11895–11971, 2007

EGU

However, even though the mean orders of magnitude are relevant, our results exhibit time discrepancies compared to the actual events, which should incriminate the local dust source accuracy for the desert area close to Liangning.

(iv) Gwangju and Osaka

Gwangju city is localized in South Korea. We display AOT and AE on Fig. 14d. The contribution of SO_4^{2-} is prominent in the simulated AOT since they contribute on average to 60% of the total mean AOT of $\tau_{Gwangju}$=0.43±0.17. BC also continuously takes a significant part in the total AOT (5 days average: 21%). The very absorbing character of BC, even compared to the SO_4^{2-}, is counterbalanced by the much higher concentrations of the latter compared to the former.

Here we note a very satisfactory agreement between modelled and AERONET AOT, in the time variations and magnitude as well. Moreover, the two dust episodes are correctly retrieved by the model. When the two dust events occur over the Korean peninsula (29 April and since 1 May), the mineral contribution to the AOT is significant and AE tends to decrease. Note the (small) contribution of coating SO_4^{2-} on dust around 12:00 UTC, 1 May (vertical black and white strips).

The same remarks are also applicable, as a whole, to our simulations in Osaka (Fig. 14e), Japan, except for the tendency observed for 1 May (here we do not have observational data). Average AOT over the 5 days is τ_{Osaka}=0.34±0.19 with values ranging between extremes of 0.09 and 0.77. With our estimates, the sulphates contribution is 71% of the average AOT over 5 days. The peak in AOT (29 to 30 April) occurs 24 h later than the same peaks modelled over the continent, due to the travel duration. Lastly, we recall that, above Osaka, the permanence of anthropogenic pollution compared to the intermittency of natural dust pollution is logically explained by the long range transport for dust whereas anthropogenic pollutants are locally produced with a constant flow.

We can thus easily give the orders of magnitude for the relative AOT contributions in BC and sulphates on the two cities located in Korea and Japan, both far away

ACPD
7, 11895–11971, 2007

EGU

from the sources of mineral pollution, but themselves sources of anthropogenic pollutants. Over 5 days, contributions of BC and sulphates are more clearly dissociated in Osaka, where on average the sulphates contribute to AOT four times more than BC (AOT_{SO4}/AOT_{BC}=0.24/0.06~4). This ratio in favour of the sulphates is also modelled in Gwangju, with, on average over five days, AOT_{SO4}/AOT_{BC}=0.26/0.09~3. Our estimates in Korea and Japan range between those of Aoki et al. (2005): AOT_{SO4}/AOT_{BC}=0.075/0.04~19, concerning the overall Japan, and the order of magnitude of AOT_{SO4}/AOT_{BC}~2, evaluated during April–May, at Tsukuba, Niigata and Sapporo cities (Japan), by Takemura et al. (2001). Lastly, we find that, even in the presence of a desert dust transported from the continent, the total average AOT at Gwangju and Osaka is mainly of anthropogenic origin, which agrees with the global assessment of Takemura et al. (2003) about the ACE-Asia area.

6 Conclusions

The objectives of our work were multiple and complementary. To sum up, we wished to develop the modelling of the cycle of the natural and anthropogenic aerosols in an area appearing increasingly implied in pollution problems, Eastern Asia. The interest of this approach is to build and to take advantage of a tool usable to study the chemical and radiative consequences of these pollutants of various origins.

In a former paper (Lasserre et al., 2005), we had built a mineral dust source according the Dust Production Model (DPM) of Marticorena and Bergametti (1995) and Marticorena et al. (1997a, b). We present the specific elements of the East-Asian desert mineral source in China and Mongolia, coupled online with the RAMS mesoscale model. This coupling enables us to simulate desert dust events, including rising, transport and the deposition (dry and wet).

Results of the study of dust plumes observed in spring 2005 over China, Korea and Japan showed the relevance of our numerical tool, for the emitted dust fluxes and the main transport features. Indeed, we model the surface concentrations and the column

load of mineral dust and the results agree with the visibility analysis, the satellite imagery and the in situ observations. In this study, we differ from most of other model works because we propose a study "in real time", and not on average over a period of at least several weeks, as the majority of other work proposes it. The limits of the model are perceptible when one seeks a perfect synchronization between results and observations, but the short-time tendencies are fairly well reproduced as a whole. The surface concentrations are in good agreement with observations in China (Hohhot and Beijing). The studies of the vertical profiles show that the dust transports take place below 3000-4000 m agl. These profiles present very quick and clear variations in structure, alternating between homogeneous and stratified forms. The model profiles above Hohhot and Beijing are confirmed by local LIDAR data of backscattering intensities and depolarisation ratio on semi quantitative grounds.

We choose aerosols (BC and sulphates) along with an anthropogenic pollution gas (SO_2, a sulphate precursor) in addition to the mineral aerosols, in order to model and to easily interpret the coexistence of these species and the consequences, mainly the optical signatures of the aerosols. For anthropogenic pollutants emissions, GEIA (BC) and EDGAR (SO_2) databases are used. Dynamic parameterizations (deposition rates) and chemistry of the anthropogenic pollutants are drastically simplified as compared to the specialized studies which we recall in the bibliography. Our parameterizations are very simple, but they are efficient enough to model the atmospheric cycles.

We describe the pollution observed on the quasi-continuum of metropoles of East China and Korea and above the seas which separate them from Japan. Maximum surface concentrations of several tens of $\mu g\,m^{-3}$ of BC and of SO_4^{2-}, and several hundreds of $\mu g\,m^{-3}$ of SO_2, are modelled over the largest cities such as Shanghai, Beijing and Seoul, in agreement with the literature data. We show moreover that the dust aerosol mix initially with the anthropogenic ones in the frontal region of the desert dust plume. Next, the mixing takes place preferentially with the mineral particles already located above the sources of anthropogenic pollution. Afterwards these mixed particles move to Japan, taking part to a pollution of continental origin.

ACPD
7, 11895–11971, 2007

Using AERONET optical measurements performed above five sites located along the aerosols pathways, we test our estimates of Aerosols Optical Thicknesses (AOT). The surface extinction for BC, sulphates (free and captured on dust) and mineral particles were derived from literature: $12\,m^2\,g^{-1}$, $8\,m^2\,g^{-1}$ and $1.2\,m^2\,g^{-1}$ respectively. The total AOT, calculated as the sum of the contributions of the four species are then compared with the AERONET AOT real time data. We also display the AERONET Angstrom Exponent (AE), which helps characterizing the nature of the aerosols. The orders of magnitude of the modelled AOT are always coherent with the orders of magnitude of the averaged observations. Especially, we retrieve a realistic evolution of AOT as compared with the AERONET time-series from 27 April to 2 May. We also show that the modelled relative abundances in aerosols are frequently compatible with the magnitudes of the AE. Such agreement of the AERONET AOT and AE suggests that our simplified tool is suitable for real-time aerosol studies in a complex environment.

Acknowledgements. Our work was supported by funding from the French Centre National de la Recherche Scientifique (Programme National de Chimie Atmosphérique). This work makes use of the RAMS model, which was developed under the support of the National Science Foundation (NSF) and the Army Research Office (ARO). Computer resources were partly provided by CINES (Centre Informatique National de l'Enseignement Supérieur). We thank B. Holben for his effort in establishing and maintaining the AERONET Dalanzadbag site. We thank Z. Li for the Liangning site AERONET data (funded through the East-Asian Study of Tropospheric Aerosols – An International Regional experiment (EAST-AIRE) project). We are also extremely grateful to I. Sano for the Osaka AERONET data and H.-B. Chen and P. Goloub for the Beijing AERONET data. The data used in this study (Fig. 4) were acquired as part of the NASA's Earth Science Enterprise. The algorithms were developed by the MODIS Science Teams. The data were processed by the MODIS Adaptive Processing System (MODAPS) and Goddard Distributed Active Archive Center (DAAC), and are archived and distributed by the Goddard DAAC. Finally, we wish to thank the computer team of the Laboratoire de Physique de l'Atmosphère (LaMP) of the Université Blaise Pascal (France): A.-M. Lanquette, S. Banson and P. Cacault.

References

Adams, J. W., Rodriguez, D., and Cox, R. A.: The uptake of SO_2 on Saharan dust: A flow tube study, Atmos. Chem. Phys. Discuss., 5, 2643–2676, 2005, http://www.atmos-chem-phys-discuss.net/5/2643/2005/.

Alfaro, S. C., Gaudichet, A., Gomes, L., and Maille, M.: Mineral aerosol production by wind erosion: Aerosol particle sizes and binding energies, Geophys. Res. Lett. 25, 991–994, 1998.

Alfaro, S. C. and Gomes, L.: Modeling mineral aerosol production by wind erosion: Emission intensities and aerosol distributions in source areas, J. Geophys. Res., 106, 18 075–18 084, 2001.

Alkezweeny, A. J. and Powell, D. C.: Estimation of transformation rate of SO_2 to SO_4 from atmospheric concentration data, Atmos. Environ., 11, 179–182, 1977.

Angström, A.: The parameters of atmospheric turbidity, Tellus, 16, 64–75, 1964.

Aoki, I., Kurosaki, Y., Osada, R., Sato, T., and Kimura, F.: Dust storms generated by mesoscale cold fronts in the Tarim Basin, Northwest China, Geophys. Res. Lett., 32, L06807, doi:10.1029/2004GL021776, 2005.

Bond, T. C. and Bergstrom R. W. : Light absorption by carbonaceous particles : An investigative review, Aerosol Sci. Tech., 40(1), 27–67, 2006.

Carmichael, G. R., Hayami, H., Calori, G., Uno, I., Cho, S. Y., Engardt, M., Kim, S.-B., Ichikawa, Y., Ikeda, Y., Ueda, H., and Amann, M.: Model Intercomparison Study of Long Range Transport and Sulfur deposition in East Asia (MICS-ASIA), Water Air Soil Poll., 130(1–4), 51–62, doi:10.1023/A:1012291200633, 2001.

Carrico, C. M., Kus, P., Rood, M. J., Quinn, P. K., and Bates, T. S.: Mixtures of pollution, dust, sea salt, and volcanic aerosol during ACE-Asia: Radiative properties as a function of relative humidity, J. Geophys. Res., 108(D23), 8650, doi:10.1029/2003JD003405, 2003.

Cautenet, G., Guillard, F., Marticorena, B., Bergametti, G., Dulac, F., and Edy, J.: Modelling of the Saharan dust event, Meteorol. Z., 9, 221–230, 2000.

Charlson, R. J., Schwartz, S. E., Hales, J. M., Cess, R. D., Coackley Jr., J.A., Hansen, J.E., and Hofmann, D.J.: Climate forcing by anthropogenic aerosols, Science, 255, 423–430, 1992.

Chin, M., Jacob, D. J., Gardner, G. M., Spiro, P. A., Foreman-Fowler, M., and Savoie, D. L.: A global three-dimensional model of tropospheric sulfate, J. Geophys. Res., 101(D13), 18 667–18 690, 1996.

Chin, M., Ginoux, P., Kinne, S., Torres, O., Holben, B. N., Duncan, B. N., Martin, R. V., Logan, J. A., Higurashi, A., and Nakajima, T.: Tropospheric Aerosol Optical Thickness from the GOCART Model and Comparisons with Satellite and Sun Photometer Measurements, J. Atmos. Sci., 59(3), 461–483, 2002.

Chin, M., Chu, A., Levy, R., Remer, L., Kaufman, Y., Holben, B., Eck, T., Ginoux, P., and Gao, Q.: Aerosol ditribution in the Northern Hemisphere during ACE-Asia: Results from global model, satllite observations, and Sun photometer measurements, J. Geophys. Res., 109, D23S90, doi:10.1029/2004JD004829, 2004.

Chylek, P., Videen, G., Nat, D., Pinnick, R. C., and Klett, J. D.: Effect of black carbon on the optical properties and climate forcing of sulfate aerosols, J. Geophys. Res., 108(16), 325–332, 1995.

Clarke, A. D., Porter, J. N., Valero, F. P. J., and Pilewskie, P.: Vertical profiles, aerosol microphysics, and optical closure during the Atlantic Stratocumulus Transition Experiment: Measured and modeled column optical properties, J. Geophys. Res., 101(D2), 4443–4454, 1996.

Clarke, A. D., Shinozuka, Y., Kapustin, V. N., Howell, S., Huebert, B., Doherty, S., Anderson, T., Covert, D., Anderson, J., Hua, X., Moore II, K. G., McNaughton, C., Carmichael, G., and Weber, R.: Size distributions and mixtures of dust and black carbon aerosol in Asian outflow: Physiochemistry and optical properties, J. Geophys. Res., 109, D15S09, doi:10.1029/2003JD004378, 2004.

Cohen, D. D., Garton, D., Stelcer, E., Hawas, O., Wang, T., Poon, S., Kim, J., Choi, B. C., Oh, S. N., Shin, H.-J., Ko, M. Y., and Uematsu, M.: Multielemental analysis and characterization of fine aerosols at several key ACE-Asia sites, J. Geophys. Res., 109, D19S12, doi:10,1029/2003JD003569, 2004.

Collins, W. D., Rasch, P. J., Eaton, B. E., Fillmore, D. W., Kiehl, J. T., Beck, C. T., and Zender, C. S.: Simulation of aerosol distributions and radiative forcing for INDOEX: Regional climate impacts, J. Geophys. Res., 107(D19), 8028, doi:10.1029/2000JD000032, 2002.

Cooke, W. F., Liousse, C., Cachier, H., and Feichter, J.: Construction of a 1°×1° fossil fuel emission data set for carbonaceous aerosol and implementation and radiative impact in the ECHAM4 model, J. Geophys. Res., 104(D22), 137–162, 1999.

Cotton, W. R., Pielke, R. A., Walko, R. L., Liston, G. E., Tremback, C. J., Jiang, H., McAnelly, R. L., Harrington, J. Y., Nicholls, M. E., Carrio, G. G., and McFadden, J. P.: Rams 2001: Current status and future directions, Meteorol. Atmos. Phys., 82, 5–29, 2003.

Cox, R. A.: Particle formation from homogeneous reactions of sulfur dioxide and nitrogen diox-

ide, Tellus, 26, 235–240, 1974.
D'Almeida, G. A., Keopke, P., and Shettle, E. P.: Atmospheric Aerosols: Global Climatology and Radiative Characteristics, AD Publishing, 559 pp, 1991.
Dubovik, O., Holben, B. N., Eck, T. F., Smirnov, A., Kaufman, Y. J., King, M. D., Tanré, D., and Slutsker, I.: Variability of Absorption and Optical Properties of Key Aerosol Types Observed in Worldwide Locations, J. Atmos. Sci., 59(3), 590–608, 2002.
Eck, T. F., Holben, B. N., Dubovik, O., Smirnov, A., Goloub, P., Chen, H. B., Chatenet, B., Gomes, L., Zhang, X.-Y., Tsay, S.-C., Ji, Q., Giles, D., and Slutsker, I.: Columnar aerosol optical properties at AERONET sites in central eastern Asia and aerosol transport to the tropical mid-Pacific, J. Geophys. Res., 110, D06202, doi:10.1029/2004JD005274, 2005.
Eliassen, A. and Saltbones, J.: Decay and transformation rates of SO_2, as estimated from emission data, trajectory and measured air concentrations, Atmos. Environ., 9, 425-429, 1975.
Fialho, P., Hansen, A. D. A., and Honrath, R. E.: Absorption coefficients by aerosols in remote areas: a new approach to decouple dust and black carbon absorption coefficients using seven-wavelength Aethalometer data, J. Aerosol Sci., 36(2), 267–282, 2005.
Guo, J., Rahn, K. A., and Zhuang, G.: A mechanism for the increase of pollution elements in dust storms in Beijing, Atmos. Environ., 38(6), 855–862, 2004.
Han, Z., Ueda, H., Matsuda, K., Zhang, R., Arao, K., Kanai, Y., and Hasome, H.: Model study on particle size segregation and deposition during Asian dust events in March 2002, J. Geophys. Res., 109, D19205, doi:10.1029/2004JD004920, 2004.
Hatakeyama, S., Murano, K., Bandow, H., Mukai, H., and Akimoto, H.: High concentration of SO_2 observed over the sea of Japan, Terr. Atmos. Ocean. Sci., 6(3), 403–408, 1995.
Hatakeyama, S., Takami, A., Wang, W., and Tang, D.: Aerial observation of air pollutants and aerosols over Bo Hai, China, Atmos. Environ., 39(32), 5893–5898, 2005.
Haywood, J., Ramaswamy, V., and Soden, B.: Tropospheric aerosol climate forcing in clear-sky satellite observations over the oceans, Science, 283, 1299–1303, 1999.
Henzing, J. S., Aerosol modelling : spatial distribution and effects on radiation. – Eindhoven : Technische Universiteit Eindhoven, 2006. – Proefschrift, 239 pp, 2006.
Holben, B. N., Eck, T. F., Slutsker, I., Tanré, D., Buis, J. P., Setzer, A., Vermote, E., Reagan, J. A., Kaufman, Y. J., Nakajima, T., Lavenu, F., Jankowiak, I., and Smirnov, A.: AERONET – A Federated Instrument Network and Data Archive for Aerosol Characterization, Remote Sens. Environ., 66, 1–16, 1998.

Huebert, B., Bertram, T., Kline, J., Howell, S., Eatough, D., and Blomquist, B.: Measurements of organic and elemental carbon in Asian outflow during ACE-Asia from the NSF/NCAR C-130, J. Geophys. Res., 109, D19S11, doi:10.1029/2004JD004700, 2004.

Jacobson, M. J.: Strong radiative heating due to the mixing state of black carbon in atmospheric aerosols, Nature, 409, 695–697, 2001.

Kalashnikova, O. V. and Sokolik, I.: Importance of shapes and compositions of wind-blown dust particles for remote sensing at solar wavelengths, Geophys. Res. Lett., 29(10), 1398, doi10.1029/2002GL014947, 2002.

Kasparian, J.: Etude de spectroscopie linéaire et non linéaire d'aérosols atmosphériques, Thèse de doctorat, Université Claude Bernard - Lyon I, 1997.

Koch, D., Jacob D., Tegen I., Rind D., and Chin M.,: Tropospheric sulfur simulation and sulfate direct radiative forcing in the GISS GCM, J. Geophys. Res., 104, 23 799–23 822, 1999.

Kristjánsson, J. E.: Studies of the aerosol indirect effect from sulfate and black carbon aerosols, J. Geophys. Res., 107(D15), 4246, doi:10,1029/2001JD000887, 2002.

Kulshrestha, M. J., Kulshrestha, U. C., Parashar, D. C., and Vairami, M.: Estimation of SO_4 contribution by dry seposition of SO_2 onto the dust particles in India, Atmos. Environ., 37(22), 3057–3063, 2003.

Kunhikrishnan, T., Lawrence, M. G., von Kuhlmann, R., Richter, A., Ladstätter-Weißenmayer, A., and Burrows, J. P.: Analysis of tropospheric NOx over Asia using the model of atmospheric transport and chemistry (MATCH-MPIC) and GOME-satellite observations, Atmos. Environ., 38(4), 581–596, 2004.

Lasserre, F., Cautenet, G., Alfaro, S. C., Gomes, L., Rajot, J.-L., Lafon, S., Gaudichet, A., Chatenet, B., Maille, M., Cachier, H., and Zhang, X. Y.: Development and validation of a simple mineral dust source inventory suitable for modelling in North Central China., Atmos. Environ., 39(21), 3831–3841, 2005.

Laurent, B., Marticorena, B., Bergametti, G., Chazette, P., Maignan, F., and Schmechtig, C.: Simulation of the mineral dust emission frequencies from desert areas of China and Mongolia using an aerodynamic roughness length map derived from the POLDER/ADEOS 1 surface products, J. Geophys. Res., 110, D18S04, doi:10.1029/2004JD005013, 2005.

Lavanchy, V. M. H., Gäggeler, H. W., Nyeki, S., and Baltensperger, U.: Elemental carbon (EC) and black carbon (BC) measurements with a thermal method and an aethalometer at the high-alpine research station Jungfraujoch, Atmos. Environ., 33(17), 2759–2769, 1999.

Li, C., Mao, J., and Lau, K.-H.: Research on air pollution in Beijing and its surroundings with

MODIS aerosol products, Optical Remote Sensing of the Atmosphere and Clouds III. Proceedings of the SPIE, Volume 4891, 419–430, 2003.
Lin, C.-Y., Wang, Z., Chen, W.-N., Chang, S.-Y., Chou, C. C. K., Sugimoto, N., and Zhao, X.: Long-range transport of Asian dust and air pollutants to Taiwan: Observed evidence and model simulation, Atmos. Chem. Phys., 7, 423–434, 2007, http://www.atmos-chem-phys.net/7/423/2007/.
Liousse, C., Cachier, H., and Jennings, S. G.: Optical and thermal measurements of black carbon aerosol content in different environments: Variation of the specific attenuation cross-section, sigma, Atmos. Environ., 27A(7), 1203–1211, 1993.
Liu, X., Zhu, J., Van Espen, P., Adams, F., Xiao, R., Dong, S., and Li, Y.: Single particle characterization of spring and summer aerosols in Beijing: Formation of composite sulfate of calcium and potassium, Atmos. Environ., 39(36), 6909–6918, 2005.
Lowenthal, D. H., Rogers, C. F., Saxena, P., Watson, J. G., and Chow, J. C.: Sensitivity of estimated light extinction coefficients to model assumptions and measurement errors, Atmos. Environ., 29(7), 751–766, 1995.
Ma, C.-J., Tohno, S., Kasahara, M., and Hayakawa, S.: Properties of individual Asian dust storm particles collected at Kosan, Korea during ACE-Asia, Atmos. Environ., 38(8), 1133–1143, 2004.
Marticorena, B. and Bergametti, G.: Modeling the atmospheric dust cycle: 1-Design of a soil derived production scheme, J. Geophys. Res., 100, 16 415–16 430, 1995.
Marticorena, B., Bergametti, G., Aumont, B., Callot, Y., N'Doumé, C., and Legrand, M.: Modeling the atmospheric dust cycle: 2-Simulations of Saharan dust sources, J. Geophys. Res., 102, 4387–4404, 1997a.
Marticorena, B., Bergametti, G., Gillette, D. A., and Belnap, J.: Factors controlling threshold friction velocity in semi-arid and arid areas of the United States, J. Geophys. Res., 102, 23 277–23 287, 1997b.
Martin, S. T., Hung H.-M., Park R. J., Jacob D. J., Spurr R. J. D., Chance K. V., and Chin M.: Effects of the physical state of tropospheric ammonium-sulfate-nitrate particles on global aerosol direct radiative, Atmos. Chem. Phys. Discuss., 3, 5399–5467, 2003, http://www.atmos-chem-phys-discuss.net/3/5399/2003/.
Martins, J. V., Artaxo, P., Liousse, C., Reid, J. S., Hobbs, P. V., and Kaufman, Y. J.: Effects of black carbon content, particle size and mixing on light absorption by aerosol particles from biomass burning in Brazil, J. Geophys. Res., 103(D24), 32 041–32 050, 1998.

Matsumoto, K., Uyama, Y., Hayamo, T., Tanimoto, H., Uno, I., and Uematsu, M.: Chemical properties of outflow patterns of anthropogenic and dust particles on Rishiri Island during the Asian Pacific Regional Characterization Experiment (ACE-Asia), J. Geophys. Res., 108(D23), 8666, doi:10.1029/2003JD003246, 2003.

McNaughton, C. S., Clarke, A. D., Howell, S. G., Moore II, K. G., Brekhovkikh, V., Weber, R. J., Orsini, D. A., Covert, D. S., Buzorius, G., Brechtel, F. J., Carmichael, G. R., Tang, Y., Eisele, F. L., Mauldin, R. L., Bandy, A. R., Thornton, D. C, and Blomquist, B.: Spatial distribution and size evolution of particles in Asian outflow: Significance of primary and secondary aerosols during ACE-Asia and TRACE-P, J. Geophys. Res., 109, D19S06, doi:10,1029/2003JD003528, 2004.

Menon, S., Hansen, J., Nazarenko, L., and Luo, Y.: Climate effects of black carbon aerosols in China and India, Science, 297(5590), 2250–2253, 2002.

Minvielle, F.: Aspects physiques et radiatifs du cycle atmosphérique des aerosols : étude numérique sur l'Océan Indien (expérience INDOEX), Thèse de doctorat (Physique de l'Atmosphère), Université Blaise Pascal (U.F.R. de Recherche Scientifique et Technique, Laboratoire de Météorologie Physique), 2003.

Minvielle, F., Cautenet, G., Andreae, M. O., Lasserre, F., Foret, G., Cautenet, S., Léon, J.-F., Mayol-Bracero, O. L., Gabriel, R., Chazette, P., and Roca, R.: Modeling the transport of aerosols during INDOEX 1999 and comparison with experimental data. Part 1: carbonaceous aerosol distribution, Atmos. Environ., 38(12), 1811–1822, 2004a.

Minvielle, F., Cautenet, G., Lasserre, F., Foret, G., Cautenet, S., Léon, J.-F., Andreae, M. O., Mayol-Bracero, O. L., Gabriel, R., Chazette, P., and Roca, R.: Modeling the transport of aerosols during INDOEX 1999 and comparison with experimental data. Part 2: continental aerosol and their optical depth, Atmos. Environ., 38(12), 1823–1837, 2004b.

Novakov, T., Chang, S. G., and Harker, A. B.: Sulfates as pollution particles: Catalytic formation on carbon (soot) particles, Science, 186, 259–261, 1974.

Olivier, J. G., Bouwman, A. F., Van der Maas, C. W. M., Berdowski, J. J. M., Veldt, C., Bloos, J. P. J., Visschedijk, A. J. H., Zandveld, P. Y. J., and Haverlag, J. L.: Description of EDGAR Version 2.0. A set of global emission inventories of greenhouse gases and ozone-depleting substances for all anthropogenic and most natural sources on a per country basis and on 1°×1° grid, RIVM/TNO report. RIVM, Bilthoven, RIVM report n. 771060 002. (TNO MEP report nr. R96/119), 1996.

Penner, J. E., Zhang, S. Y., Chin, M., Chuang, C. C., Feichter, J., Feng, Y., Geogdzhayev, I.

V., Ginoux, P., Herzog, M., Higurashi, A., Koch, D., Land, C., Lohmann, U., Mishchenko, M., Nakajima, T., Pitari, G., Soden, B., Tegen, I., and Stowe, L.: A Comparison of model- and satellite-derived aerosol optical depth and reflectivity, J. Atmos. Sci., 59(3), 441–460, 2002.

Pradelle, F. and Cautenet, G.: Radiative and microphysical interactions between marine stratocumulus clouds and Saharan dust 2. Modeling, J. Geophys. Res., 107(D19), 4413, doi:10.1029/2000JD000156, 2002.

Pryor, S. C., Simpson, R., Guise-Bagley, L., Hoff, R., and Sakiyama, S.: Visibility and Aerosol Composition in the Fraser Valley During REVEAL, J. Air Waste Manage. Assoc., 47, 147–156, 1997.

Qiu, J. and Yang, L.: Variation characteristics of atmospheric aerosol optical depths and visibility in North China during 1980-1994, Atmos. Environ., 34, 603–609, 2000.

Quinn P. K., Coffman, D. J., Bates, T. S., Miller, T. L., Johnson, J.E., Voss, K., Welton, E. J., Neususess, C.: Dominant aerosol chemical components and their contribution to extinction during the Aerosols99 cruise across the Atlantic, J. Geophys. Res., 106(D18), 20 783-20 809, 2001.

Reddy, M. S., Boucher, O., Balkanski, Y., and Schultz, M.: Aerosol optical depths and direct radiative perturbations by species and source type, Geophys. Res. Lett., 32, L12803, doi:10.1029/2004GL021743, 2005.

Ricard, V.: Aérosols dans l'arctique européen: sources, transformations et propriétés optiques, Thèse de doctorat, CNRS-Université Joseph Fourier (Grenoble-I), Laboratoire de Glaciologie et géophysique de l'Environnement, 2001.

Roelofs, G. J., Kasibhatla, P., Barrie, L., Bergmann, D., Bridgeman, C., Chin, M., Christensen, J., Easter, R., Feichter, J., Jeunken, A., Kjellström, E., Koch, D., Land, C., Lohmann, U., and Rasch, P.: Analysis of regional budgets of sulfur species modeled for the COSAM exercise, Tellus, 53B, 5, 673–64, 2001.

Sano, I., Mukai, S., Okada, Y., Holben, B. N., Ohta, S., and Takamura, T.: Optical properties of aerosol during APEX and ACE-Asia experiments, J. Geophys. Res., 108(D23), 8649, doi:10.1029/2002JD003263, 2003.

Sato, M., Hansen, J., Koch, D., Lacis, A., Ruedy, R., Dubovik, O., Holben, B. N., Chin, M., and Novakov, T.: Global atmospheric black carbon inferred from AERONET, P. Natl. Acad. Sci. USA, 100(11), 6319–6324, 2003.

Schuster G. L.: inferring the specific absorption and concentration of black carbon from aeronet aerosol retrievals, PhD thesis, Pennsylvania State University, Graduate School, Department

of Meteorology, 85 pp, 2004.
Seinfeld, J. H. and Pandis, S. N.: Atmospheric chemistry and physics: From air pollution to climate change, Wiley, New York, 1326 pp, 1998.
Shi, Z. B., Shao, L. Y., Jones, T. P., Whittaker, A. G., Lu, S. L., Berube, K. A., He, T. O., and Richards, R. J.: Characterization of airborne individual particles collected in an urban area, a satellite city and a clean air area in Beijing, 2001. Atmos. Environ., 37(29), 4097–4108, 2003.
Shimizu, A., Sugimoto, N., Matsui, I., Arao, K., Uno, I., Murayama, T., Kagawa, N., Aoki, K., Uchiyama, A., and Yamazaki, A.: Continuous observations of Asian dust and other aerosols by polarization lidars in China and Japan during ACE-Asia, J. Geophys. Res., D19S17, doi:10.1029/2002JD003253, 2004.
Smirnov, A., Holben, B. N., Dubovik, O., O'Neill, N. T., Eck, T. F., Westphal, D. L., Goroch, A. K., Pietras, C., and Slutsker, I.: Atmospheric aerosol optical properties in the Persian Gulf, J. Atmos. Sci., 59(3), 620–634, 2002.
Solmon, F., Giorgi, F., and Liousse, C.: Aerosol modelling for regional climate studies: application to anthropogenic particles and evaluation over a European/African domain, Tellus, 58B, 51–72, 2006.
Sun, J. M., Zhang, M., and Liu, T. S.: Spatial and temporal characteristics of dust storms in China and its surrounding regions, 1960-1999: Relations to source area and climate, J. Geophys. Res., 106(D10), 10 325–10 333, 2001.
Sun, Z., Wang, X., and Zeng, X.: Radiative Forcing of SO_2 and NO_x: A Case Study in Beijing. Adv. Atmos. Sci., 23(2), 317–322, 2006.
Ta, W., Wang, T., Honglang, X., Xueyi, Z., and Zhen, X.: Gaseous and particulate air pollution in the Lanzhou Valley, China, Sci. Total Environ., 320(2–3), 163–176, 2004.
Takemura, T., Nakajima, T., Nozawa, T., and Aoki, K.: Simulation of future aerosol distribution, radiative forcing, and long-range transport in east Asia, J. Meteor. Soc. Jpn, 79(6), 1139–1155, 2001.
Takemura, T., Nakajima, T., Dubovik O., Holben B. N., and Kinne S.: Single-Scattering Albedo and Radiative Forcing of Various Aerosol Species with a Global Three-Dimensional Model, J. of Climate, 15(4), 333—352, 2002.
Takemura, T., Nakajima, T., Higurashi, A., Ohta, S., and Sugimoto, N.: Aerosol distributions and radiative forcing over the Asian Pacific region simulated by Spectral Radiation Transport Model for Aerosol Species (SPRINTARS), J. Geophys. Res., 108(D23), 8659,

doi:10.1029/2002JD003210, 2003.
Tang, Y., Carmichael, G. R., Kurata, G., Uno, I., Weber, R. J., Song, C.-H., Guttikunda, S. K., Woo, J.-H., Streets, D. G., Wei, C., Clarke, A. D., Huebert, B., and Anderson, T. L.: Impacts of dust on regional tropospheric chemistry during the ACE-Asia experiment: A model study with observations, J. Geophys. Res., 109, D19S21, doi:10,1029/2003JD003806, 2004.
Tegen, I. and Fung, I.: Contribution to the mineral aerosol load from land surface modification, J. Geophys. Res., 100(D9), 18 707–18 726, 1995.
Tegen, I., Koch, D., Lacis, A. A., and Sato, M.: Trends in tropospheric aerosol loads and corresponding impact on direct radiative forcing between 1950 and 1990: A model study, J. Geophys. Res., 105(D22), 26971–26990, 2000.
Trijonis, J. C., Maim, W. C., Pitchford, M., White, W. H., Charlson, R. J., and Husar, R.: Visibility: Existing and Historical Conditions – Causes and Effects. Acidic Deposition: State of Science and Technology Report No. 24, National Acid Precipitation Assessment Program, Washington, D.C., 1990.
Uno, I., Carmichael, G. R., Streets, D., Satake, S., Takemura, T., Woo, J.-H., Uematsu, M., and Ohta, S.: Analysis of surface black carbon distributions during ACE-Asia using a regional-scale aerosol model, J. Geophys. Res., 108(D23), 8636, doi:10.1029/2002JD003252, 2003.
Van Dingenen, R., Putaud, J.-P., Martins-Dos Santos S., and Raes F.: Physical aerosol properties and their relation to air mass origin at Monte Cimone (Italy) during the first MINATROC campaign, Atmos. Chem. Phys. Discuss., 5, 1067–1114, 2005, http://www.atmos-chem-phys-discuss.net/5/1067/2005/.
Wang, C.: A modeling study on the climate impacts of black carbon aerosols, J. Geophys. Res., 109, D03106, doi:10.1029/2003JD004084, 2004.
Wang, G., Bai, J., Kong, Q., and Emilenko, A.: Black Carbon particles in the urban atmosphere in Beijing, Adv. Atmos. Sci., 22(5), 640–646, 2005.
Wang, T., Wong, C. H., Cheung, T. F., Blake, D. R., Arimoto, R., Baumann, K., Tang, J., Ding, G. A., Yu X. M., Li, Y. S., Streets, D. G., and Simpson, I. J.: Relationships of trace gases and aerosols and the emission characteristics at Lin'an, a rural site in eastern China, during spring 2001, J. Geophys. Res., 109, D19S05, doi:10,1029/2003JD004119, 2004.
Wang, Y., Zhuang, G., Zhang, X., Huang, K., Xu, C., Tang, A., Chen, J., and An, Z.: The ion chemistry, seasonal cycle, and sources of PM2.5 and TSP aerosol in Shanghai, Atmos. Environ., 40(16), 2935–2952, 2006.
Watson, J. G., Chow, J. C., Lowenthal, D. H., Cahill, C. F., Blumenthal, D. L., Richards, L.

W., and Jorge, H.G.: Aerosol chemical and optical properties during the Mt. Zirkel Visibility Study. J. Environ. Qual., 30(4), 1118–1125, 2001.
Wu, J., Jiang, W., Fu, C., Su, B., Liu, H., and Tang, J.: Simulation of the radiative effect of Black Carbon aerosols and the regional climate responses over China, Adv. Atmos. Sci., 21(4), 637–649, 2004.
Xia, X.-A., Chen, H.-B., Wang, P.-C., Zong, X.-M., Qiu, J.-H., and Goulomb, P.: Aerosol properties and their spatial and temporal variations over North China in spring 2001, Tellus, 57(B), 28–39, 2005.
Xu, X., Gao, J., Dockery, D. W., and Chen, Y.: Air pollution and daily mortality in residential areas of Beijing, China, Arch. Environ. Health, 49(4), 216–222, 1994.
Xu, Y. and Carmichael, G. R.: Modeling the dry deposition velocity of sulfur dioxide and sulfate in Asia, J. Appl. Meteorol., 37(10), 1084–1099, 1998.
Xu, J., Bergina, M. H., Yuc, X., Liuc, G., Zhaob, J., Carricoa, C. M., and Baumann, K.: Measurement of aerosol chemical, physical and radiative properties in the Yangtze delta region of China, Atmos. Env., 36, 161—173, 2002.
Yang, J., Wang, J., Cao, D., Ge, C., and Gao, S.: Pollution control strategy based on performance in power sector, CRAES Research Report, 2002.
Yao, X., Chan, C. K., Fang, M., Cadle, S., Chan, T., Mulawa, P., He, K., and Ye, B.: The water-soluble ionic composition of PM2.5 in Shanghai and Beijing, China, Atmos. Environ., 36(26), 4223–4234, 2002.
Yao, X., Lau, A. P. S., Fang, M., Chan, C. K., and Hu, M.: Size distributions and formation of ionic species in atmospheric particulate pollutants in Beijing, China: 1-Inorganic ions, Atmos. Environ., 37(21), 2991–3000, 2003.
Yu, J., Guinot, B., Yu, T., Wang, X., and Liu, W.: Seasonal variations of number size distributions and mass concentrations of atmospheric particles in Beijing, Adv. Atmos. Sci., 22(3), 401–407, 2005.
Zhang, D., Zang, J., Shi, G., Iwasaka, Y., Matsuki, A., and Trochkine, D.: Mixture state of individual Asian dust particles at a coastal site of Qingdao, Atmos. Environ., 37(28), 3895–3901, 2003.
Zhang, D., Iwasaka, Y., Shi, G., Zang, J., Hu, M., and Li, C.: Separated status of the natural dust plume and polluted air masses in an Asian dust storm event at coastal areas of China, J. Geophys. Res., 110, D06302, doi:10.1029/2004JD005305, 2005.
Zhang, X. Y., Gong, S. L., Shen, Z. X., Mei, F. M., Xi, X. X., Liu, L. C., Zhou, Z. J., Wang, D.,

Wang, Y. Q., and Cheng, Y.: Characterization of soil dust aerosol in China and its transport and distribution during 2001 ACE-Asia: 1. Network observations, J. Geophys. Res., 108(D9), 4261, doi:10.1029/2002JD002632, 2003b.

Zhang, X. Y., Gong, S. L., Zhao, T. L., Arimoto, R., Wang, Y. Q., and Zhou, Z. J.: Sources of Asian dust and role of climate change versus desertification in Asian dust emission, Geophys. Res. Lett., 30(24), 2272, doi:10.1029/2003GL018206, 2003c.

Zhang, Y., Zhu, X., Slanina, S., Shao, M., Zeng, L., Hu, M., Bergin, M., and Salmon, L.: Aerosol pollution in some Chinese cities (IUPAC Technical Report), Pure Appl. Chem., 76(6), 1227–1239, 2004b.

Table 1. Magnitudes of mineral dust mass production, inside zones 1, 2 and 3, since 27 April, 00:00 UTC to 2 May, 00:00 UTC, 2005.

Zone	Geographic coordinates	Total mass produced during 5 days (Mt)	Mass maximum produced during 3 h (Mt)	Average of the masses produced during 3 h (Mt)	Standard deviation of the masses produced during 3 h (Mt)
1	(40–45 N, 100–109 E)	1.27	0.259 (27, 06:00 UT)	0.031	0.051
2	(42–47 N, 110–119 E)	1.20	0.090 (29, 03:00 UT)	0.029	0.023
3	(38–50 N, 94–119 E)	5.50	0.456 (27, 06:00 UT)	0.134	0.111

Table 2. Summary statistics of the modelled surface concentrations, since 27 April, 00:00 UTC, to 2 May, 00:00 UTC, 2005, for Hohhot and Beijing cities.

Volume concentrations	Hohhot				Beijing			
Statistics ($\mu g\,m^{-3}$)	Mineral dust	SO_2	SO_4^{2-}	BC	Mineral dust	SO_2	SO_4^{2-}	BC
Average	235	4.15	1.09	1.07	188	37.2	4.05	4.00
Standard deviation	183	5.28	1.80	0.74	123	23.4	5.32	2.49
Minimum	13	0.31	0.02	0.26	59	5.58	0.15	0.68
Maximum	715	21.5	7.64	3.03	618	85.0	18.30	9.45

ACPD
7, 11895–11971, 2007

Table 3. Specific extinction sections for mineral dust ($\sigma_{d\text{ext}}$), sulphates (σ_{SO4ext}) and BC ($\sigma_{BC\text{ext}}$) according to the literature, for various relative humidity and wavelengths.

Mineral dust		*Sulphates*		*BC*	
$\sigma_{dust\ ext}$ (m^2g^{-1})	references *(comments)*	$\sigma_{SO4\ ext}$ (m^2g^{-1})	references *(comments)*	$\sigma_{BC\ ext}$ (m^2g^{-1})	references *(comments)*
0.6 ~ 1.25	Trijonis et al. (1990) *(Fine ~ Coarse)*	2.5 ~ 3.0	Trijonis et al. (1990)	10.5	Trijonis et al. (1990)
0.2 ~ 0.4 1.0 ~ 2.0	Tegen and Fung (1995) *(1-10 µm)* *(<1 µm)*	2.5 ~ 7.5	Charlson et al. (1992)	14 ~ 25	Liousse et al. (1993) *(urban)*
0.9 ~ 1.3	Clarke et al. (1996)	5 ~ 16	Clarke et al. (1996)	5 ~ 20	Pryor et al. (1997)
0.08 ~ 1.70 0.09 ~ 4.77 0.14 ~ 3.29	Haywood et al. (1999)	5 ~ 12	Chin et al. (1996)	9	Seinfeld et Pandis (1998)
		8.4	Koch et al. (1999)	5 ~ 22	Martins et al. (1998)
		2.6 ~ 5.8	Quinn et al. (2001)	5.0 ~ 9.3	Lavanchy et al. (1999)
		2.5	Watson et al. (2001) *("quasi"-dry scattering)*	11	Cooke et al. (1999)
		7.35 ~ 12.2 *(44 if RH>99%)*	Penner et al. (2002) *(ref. included)*	10	Tegen et al. (2000)
2.9 ~ 4.1 0.4 ~ 0.6	Quinn et al. (2001) *(<1 µm)* *(>1 µm)*	11	Chin et al. (2002)	8.9 ~ 10	Penner et al. (2002) *(ref. included)*
1.76	Watson et al. (2001) *("quasi"-dry scattering)*	4.28 ~ 20.09	Takemura et al. (2002) *(RH: 0%~90%)*	12	Chin et al. (2002)
0.8	Chin et al. (2002)	4.6 ~ 17.7	Martin et al. (2003) *(RH:low~80%)*	5 ~ 9	Clarke et al. (2004)
0.017 ~ 1.303	Collins et al. (2002)			8.6 (7.0)	Xu et al. (2002) *(std deviation)*
~ 0.009 ~ 0.3	Clarke et al. (2004) *(absorption)* *(scattering)*			6.3 ~ 8.7	Bond and Bergstrom (2006)
				7.7 ~ 12.5	Schuster (2004)
				8.5 ~ 19	Van Dingenen et al. (2005)
				6.4 ~ 10.9	Henzing (2006)
				9.6 ~ 14.6 12.1 ~ 20.2	Solmon et al. (2006) *(0.06 µm)* *(0.1 µm)*

ACPD
7, 11895–11971, 2007

EGU

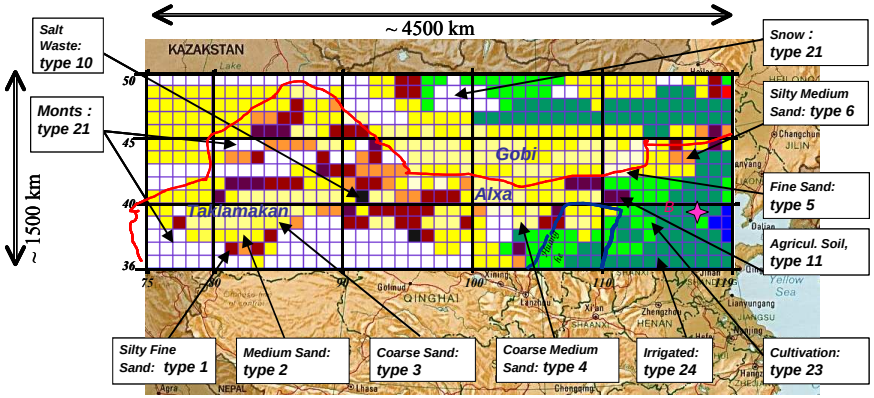

Fig. 1. Map of the DPM soil types, for North China and Mongolia. Codes are the typology of Marticorena and Bergametti (1997) and are shown on some places. The red line indicates the Northern China border, B (star): Beijing. Blue line: roughly indicates the Huang He River. Gobi desert, Alxa plateau and Taklamakan desert are localised.

ACPD
7, 11895–11971, 2007

EGU

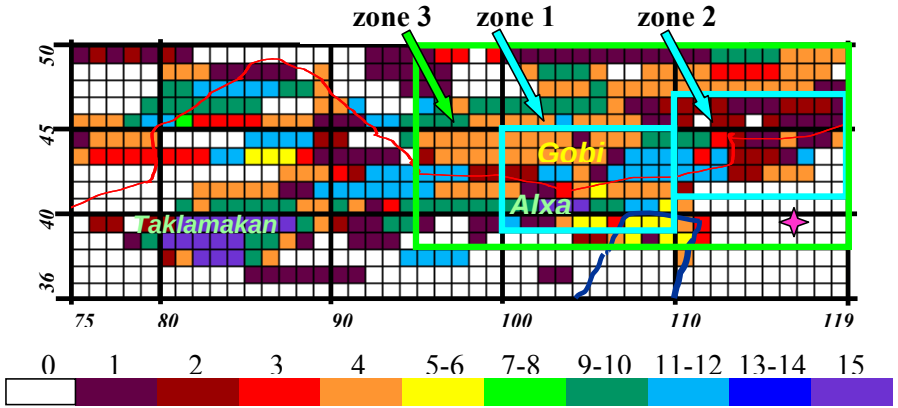

Fig. 2. Map of the DPM erodibilities (expressed as %), April 2005, for the same areas as Fig. 1. "zone 1", "zone 2" and "zone 3" are localised.

ACPD
7, 11895–11971, 2007

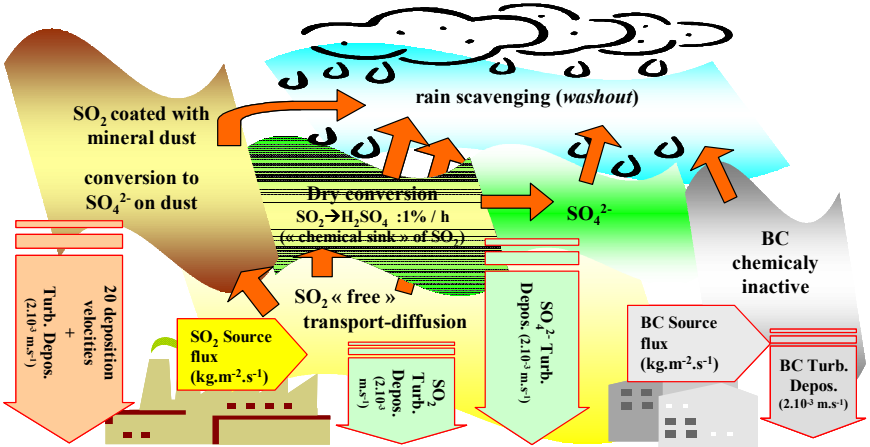

Fig. 3. Processes for sulphur compounds, mineral dust and BC used in the simplified model of transports and captures.

ACPD
7, 11895–11971, 2007

EGU

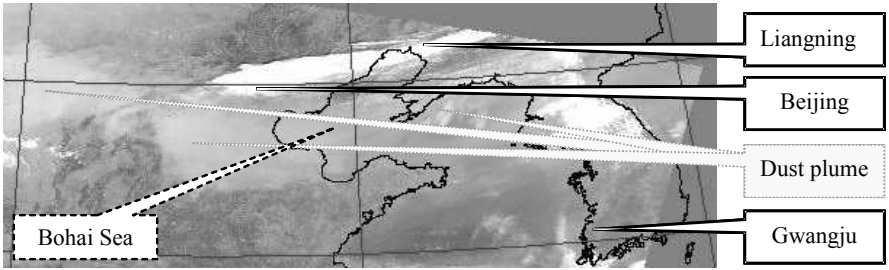

Fig. 4. Part of MODIS satellite imagery of 28 April 2005, 03:00 UTC, showing the mineral dust plume of mineral dust above North East China. Beijing, Liangning and Gwangju cities are localised.

ACPD
7, 11895–11971, 2007

EGU

Fig. 5. Composite locating AERONET sites used to roughly estimate the species of the aerosols present over NE China since 28 April to 2 May 2005. Hohhot city is localised. These AERONET sites are also used to precisely valid the modelled AOT.

ACPD
7, 11895–11971, 2007

EGU

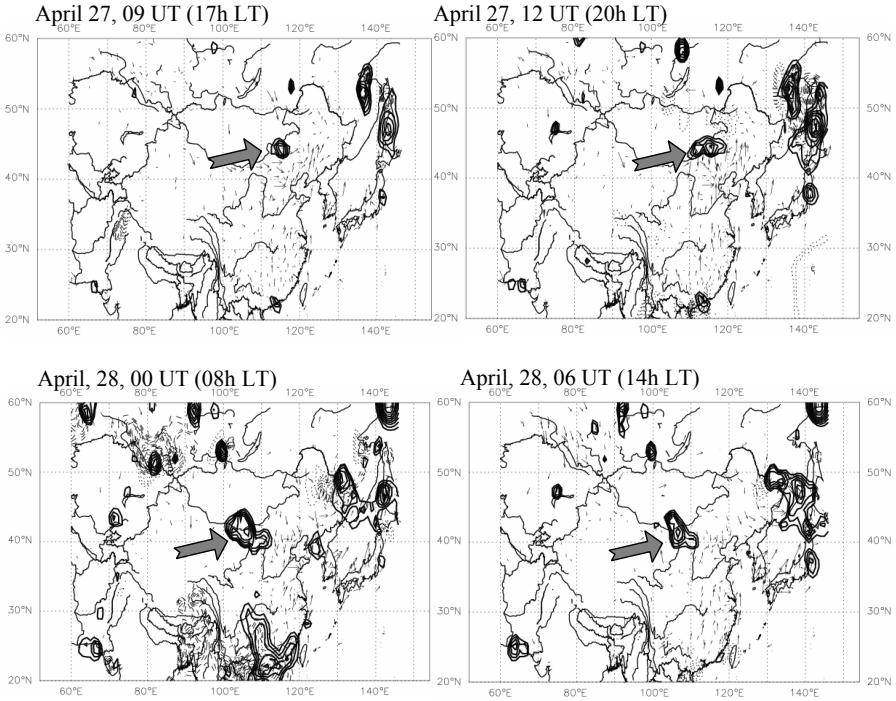

Fig. 6a. Changes of relative visibilities interpolated in Asia for 27 April and 28 April 2005. Thick lines: decreasing of more than 50%; Thin lines: rainfall (arbitrary units); Thin doted lines: RH>80% (a.u.); vectors: wind (a.u.); large arrows locate the main area of interest.

ACPD
7, 11895–11971, 2007

EGU

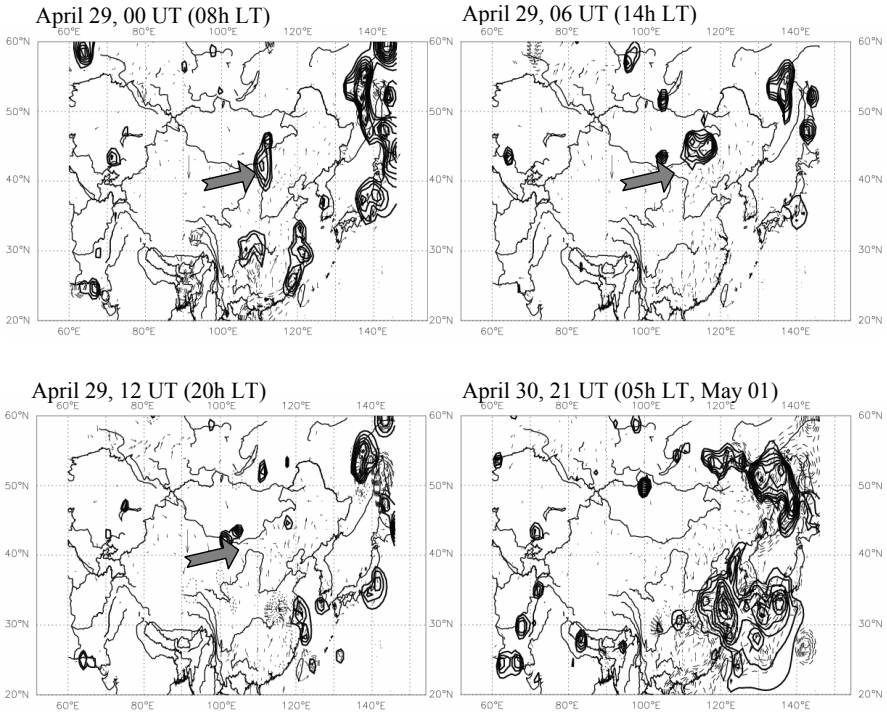

Fig. 6b. See Fig. 6a, for 29 April and 30 April 2005.

ACPD
7, 11895–11971, 2007

EGU

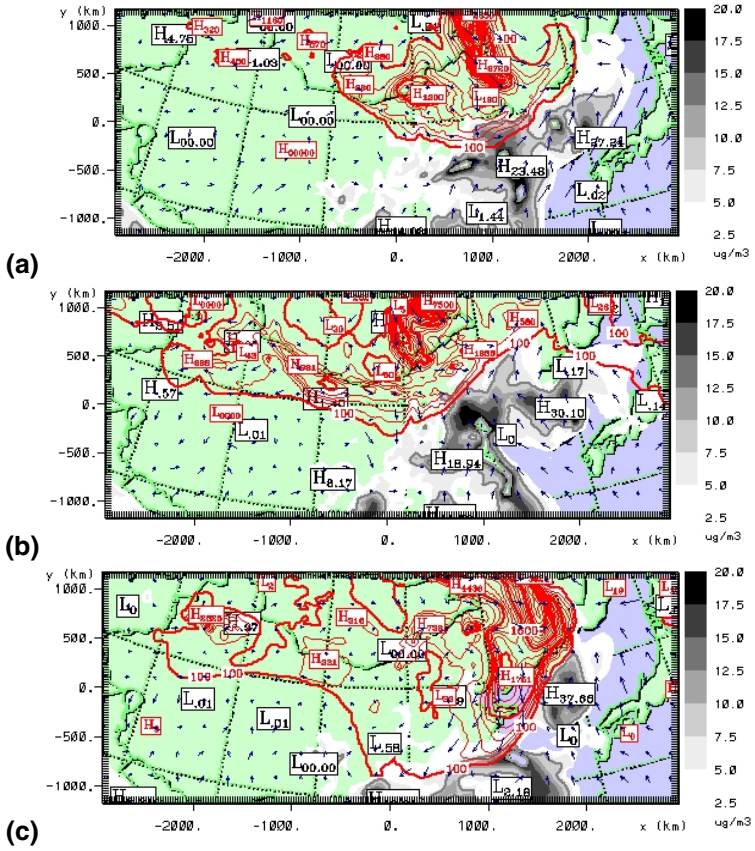

Fig. 7. Isocontours of surface BC concentrations ($\mu g\,m^{-3}$, grey-coloured and black labels: H means maximum and L means minimum) and of surface mineral dust concentrations (red-coloured and labels). Blue arrows: surface winds (a.u.). Model results at 00:00 UTC (08:00 LT) on 28 April **(a)**, 30 April **(b)** and 1 May **(c)**, 2005.

ACPD
7, 11895–11971, 2007

EGU

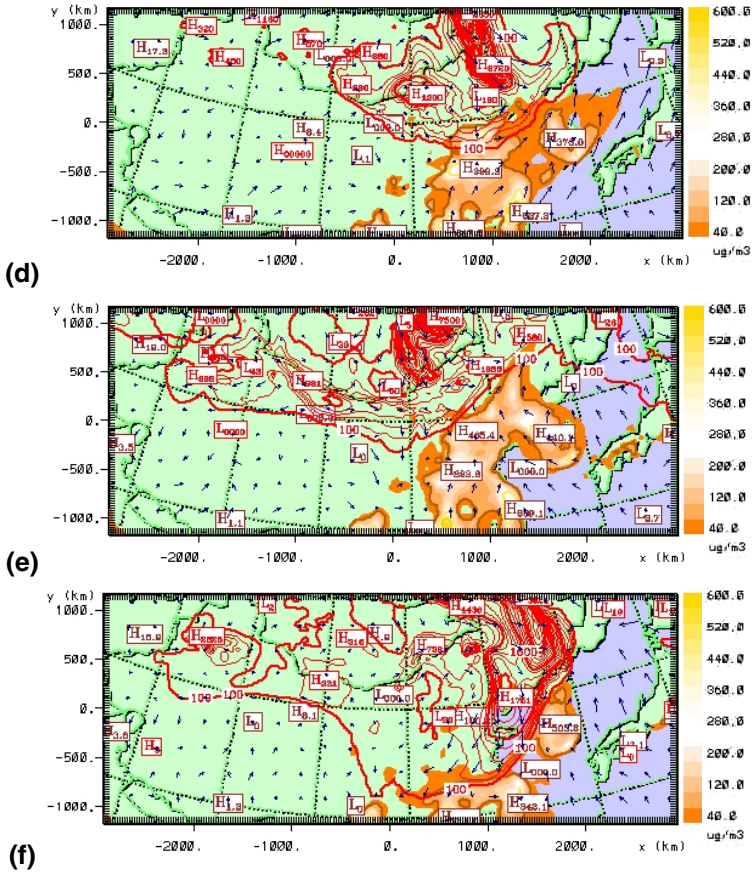

Fig. 7. Isocontours of surface SO_2 concentrations ($\mu g\,m^{-3}$, orange-coloured and brown labels: H means maximum and L means minimum) and of surface mineral dust concentrations (red-coloured and labels). Blue arrows: surface winds (a.u.). Model results at 00:00 UTC (08:00 LT) on 28 April **(d)**, 30 April **(e)** and May 1 **(f)**, 2005.

ACPD
7, 11895–11971, 2007

EGU

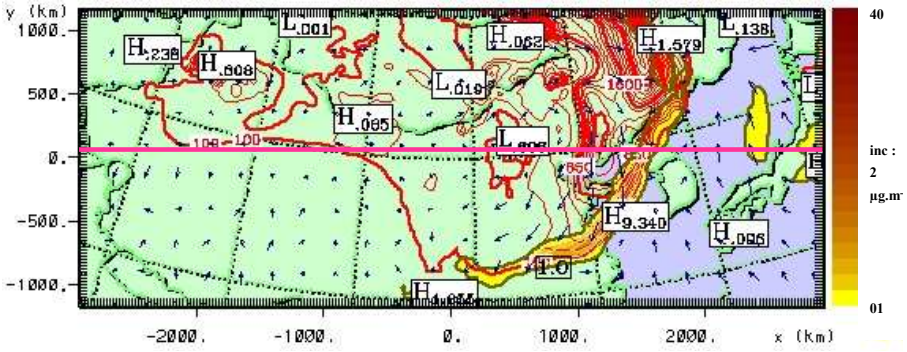

Fig. 8a. Isocontours of surface "captured" SO_2 concentrations ($\mu g\,m^{-3}$, yellow-coloured and black labels: H means maximum and L means minimum) and of surface mineral dust concentrations (red-coloured and labels). Blue arrows: surface winds (a.u.). Model results at 00:00 UTC (08:00 LT) for 1 May 2005.

ACPD
7, 11895–11971, 2007

EGU

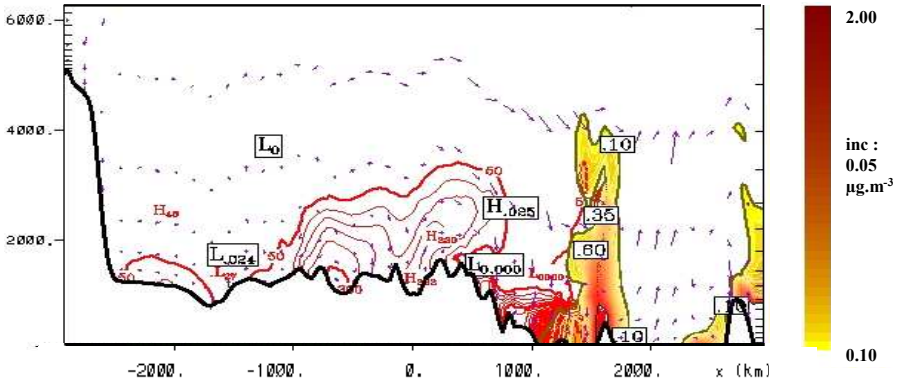

Fig. 8b. Isocontours of vertical "captured" SO_2 concentrations and of vertical mineral dust concentrations as Fig. 8a, but with vertical zonal cross-section (along pink line of Fig. 8a).

ACPD

7, 11895–11971, 2007

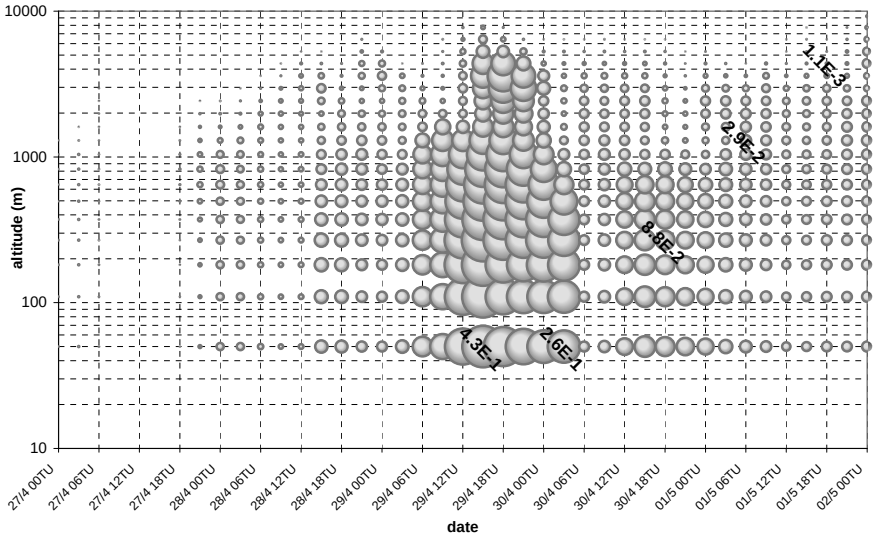

Fig. 9. Symbolic intercomparaison of the "captured" SO_2 concentrations (grey spheres): time series (UTC) of the vertical distributions (altitudes: logarithmic scale) above Beijing.

ACPD
7, 11895–11971, 2007

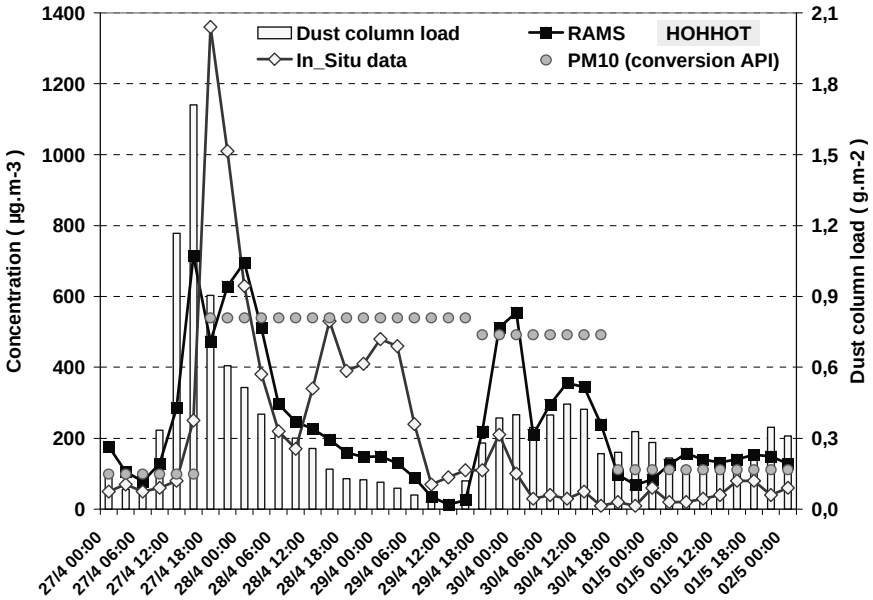

Fig. 10a. Time series of the surface mineral dust concentrations ($\mu g\,m^{-3}$) and of vertical integrated column load ($g\,m^{-2}$) at Hohhot: model concentrations (black squares); in situ observed concentrations (diamonds); PM_{10} concentrations from API data (grey circles); model column loads (bar charts).

ACPD
7, 11895–11971, 2007

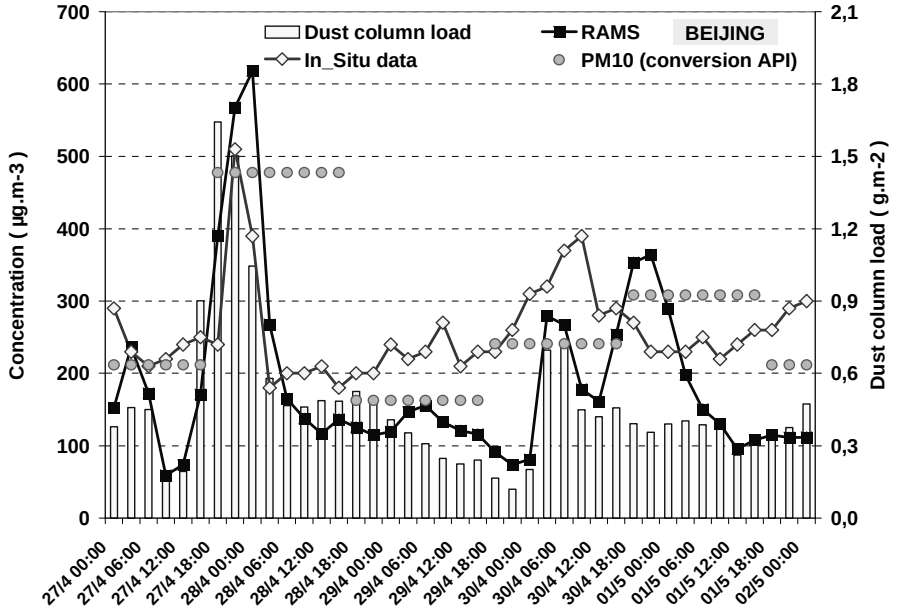

Fig. 10b. See Fig. 10a, for Beijing.

ACPD
7, 11895–11971, 2007

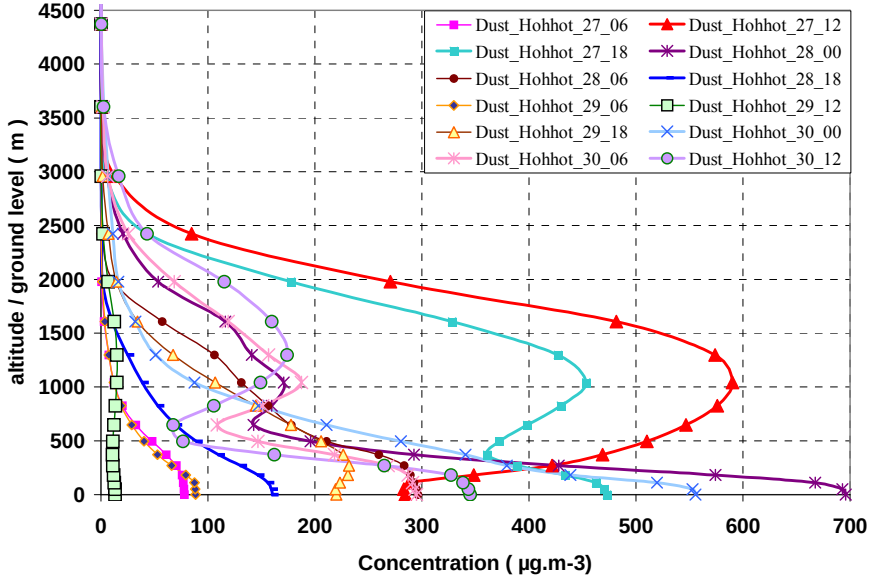

Fig. 11a. Time vertical profiles of dust concentrations ($\mu g\,m^{-3}$), between surface and 4500 m above Hohhot (UTC hours).

ACPD
7, 11895–11971, 2007

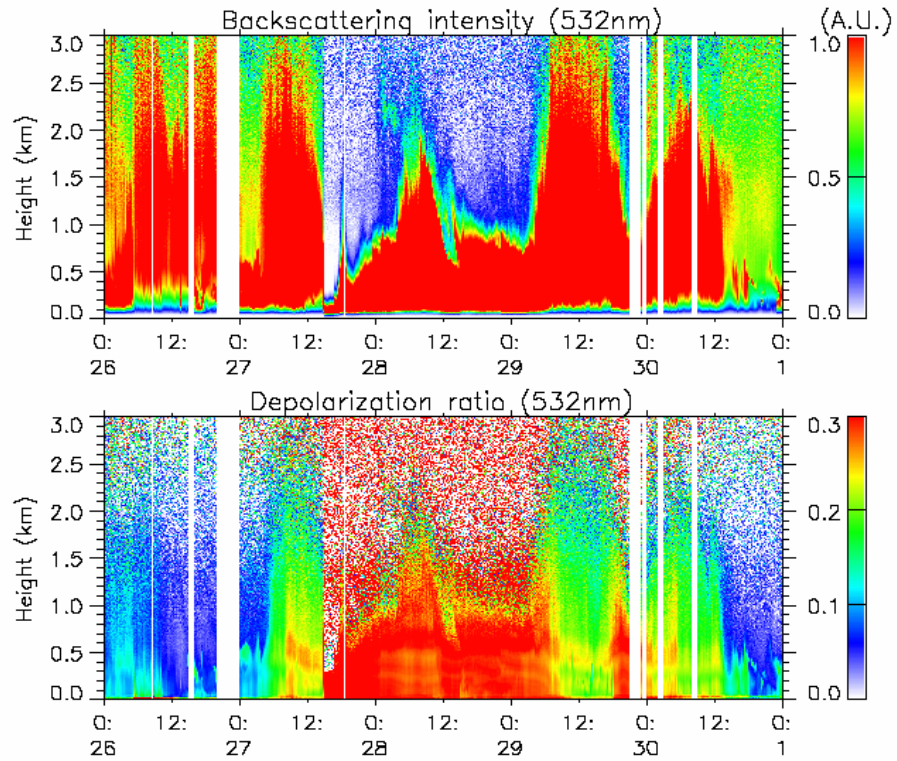

Fig. 11b. See Fig. 11a, for Beijing.

ACPD
7, 11895–11971, 2007

EGU

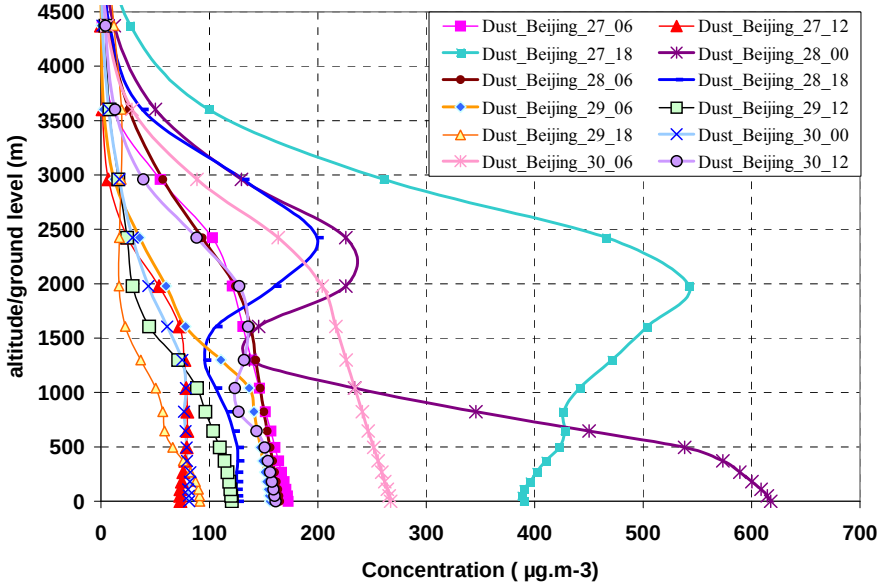

Fig. 12a. Hohhot Lidar measurements (532 nm) since April 26, 00:00 UTC, to 1 May, 00:00 UTC, 2005: – top: Backscattering Intensities (a.u.) – bottom: Depolarisation Ration.

ACPD
7, 11895–11971, 2007

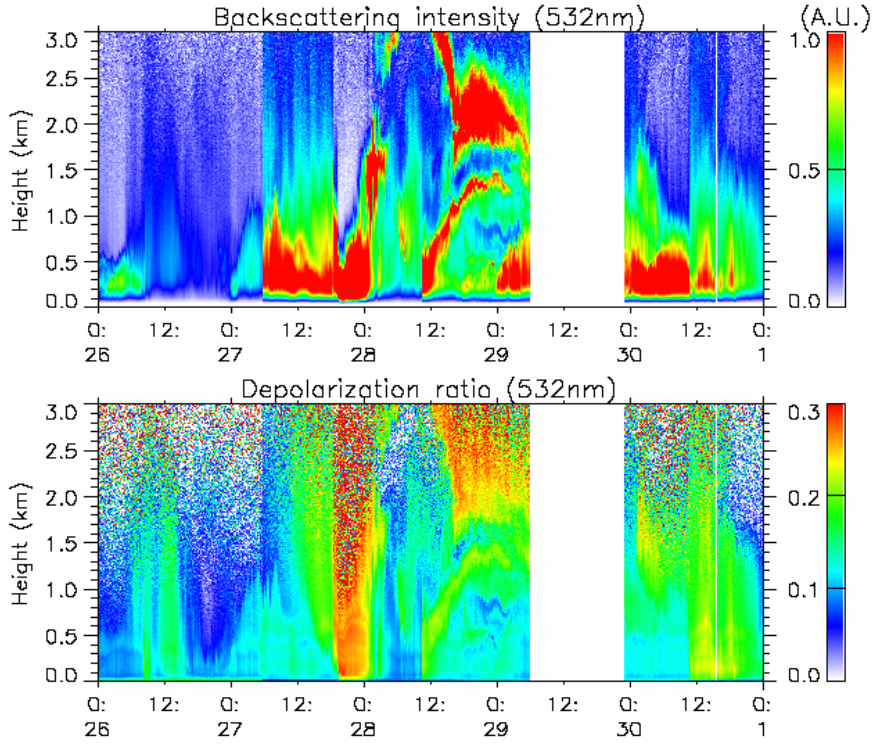

Fig. 12b. See Fig. 12a, for Beijing.

ACPD
7, 11895–11971, 2007

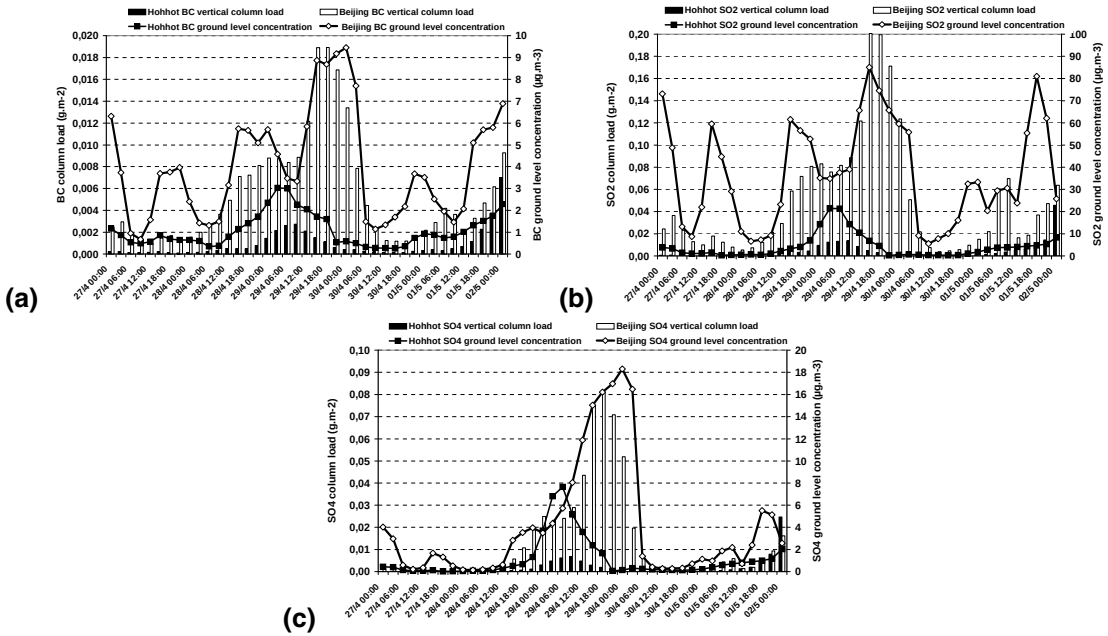

Fig. 13. Time series, since 27 April, 00:00 UTC, to 2 May, 00:00 UTC, 2005, of modelled surface concentration ($\mu g\,m^{-3}$: specific scale on the right, for each specie) and of column load ($g\,m^{-2}$: specific scale on the left, for each specie), at Hohhot (black squares and bar charts) and Beijing (white diamonds and bar charts), for the three anthropogenic species: BC **(a)**, SO_2 **(b)** and Sulphates **(c)**.

ACPD
7, 11895–11971, 2007

EGU

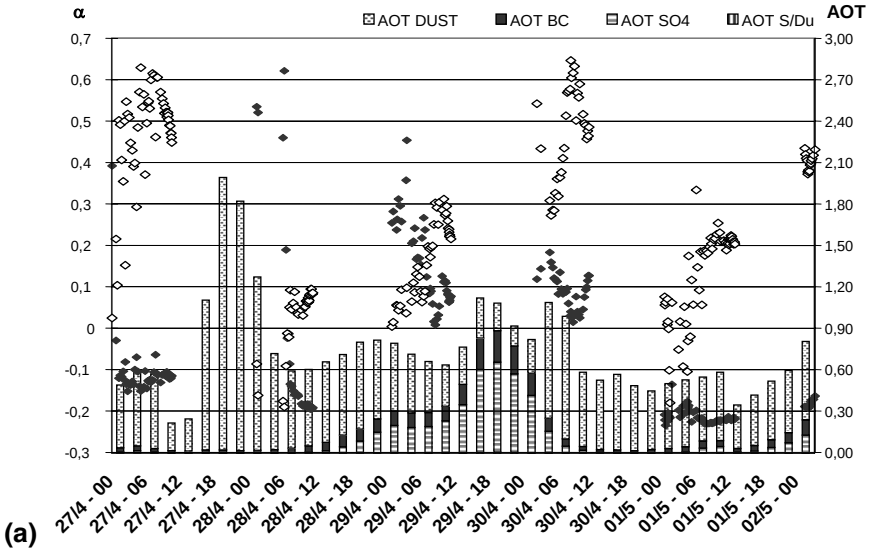

Fig. 14. Time series, since 27 April, 00:00 UTC, to 2 May, 00:00 UTC, 2005, of modelled AOT, with respectives AOT contributions of mineral dust (light grey columns with points, top of total columns if present), BC (dark grey columns), SO_4^{2-} (horizontal grey and white stripes) and "captured" SO_2 (vertical stripes, far from visible on the 3 sites of China/Mongolia). Also displayed: AERONET AOT (black diamonds, right scale, common to the modelled AOT) and Angstrom Exponent α (white diamonds, left scale). Results for Beijing (China **a**), Dalanzadgad (Mongolia **b**), Liangning (China, **c**), Gwangju (Korea, **d**) and Osaka (Japan, **e**), with specific scales for each site.

ACPD
7, 11895–11971, 2007

EGU

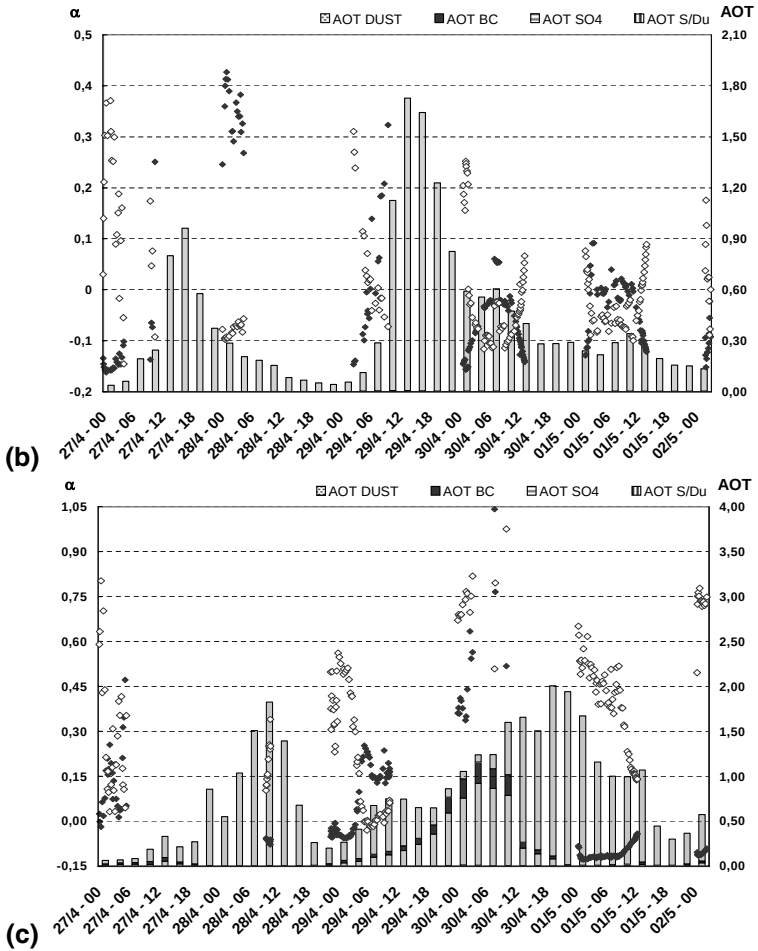

Fig. 14. Continued.

ACPD
7, 11895–11971, 2007

EGU

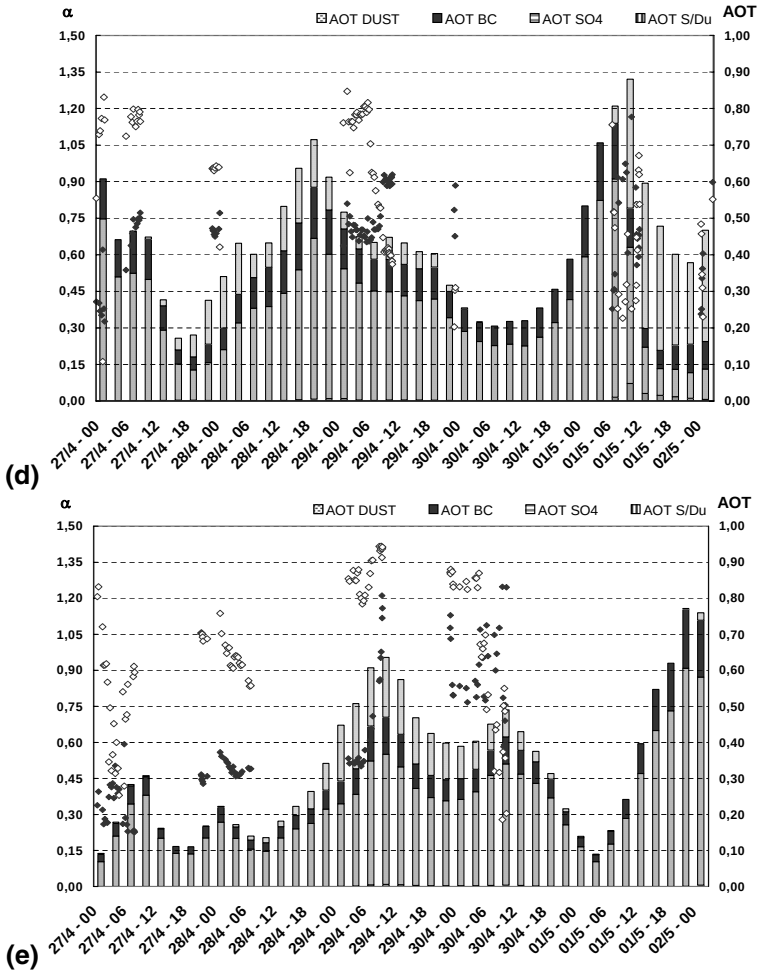

Fig. 14. Continued.

ACPD
7, 11895–11971, 2007

EGU